Mine Neutralization Exercise (MINEX) Sound Measurement Trial

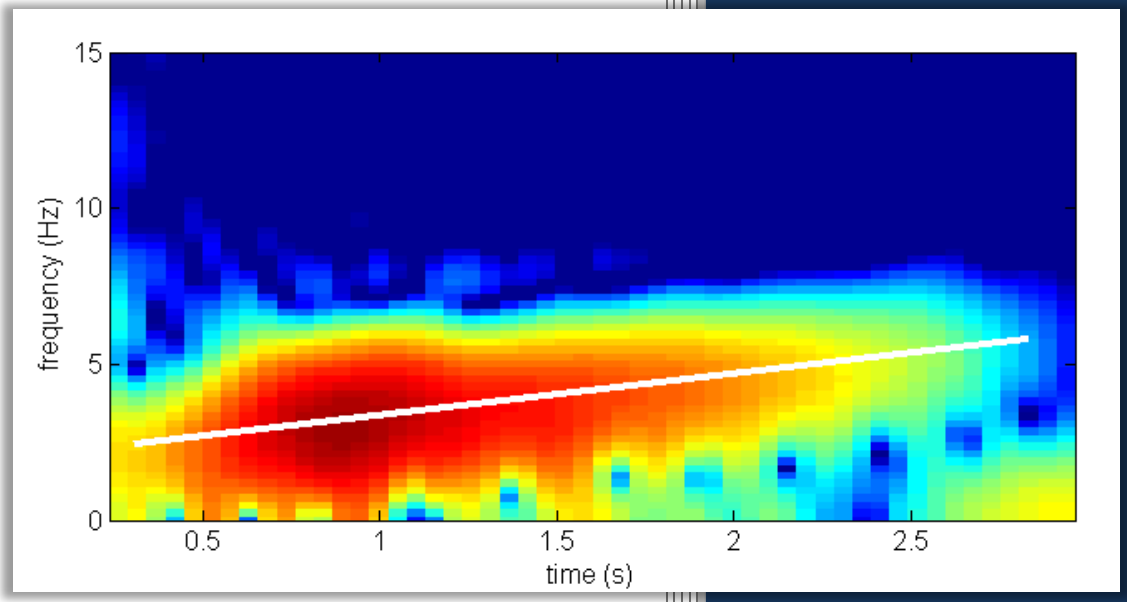

Submitted to:

Naval Facilities Engineering Command Atlantic under
HDR Environmental, Operations and Construction, Inc.
Contract No. N62470-10-D-3011, Task Order 03

Prepared By:

Alexander G. Soloway
Dept. of Mechanical Engineering,
University of Washington,
Seattle, Washington

Peter H. Dahl
Applied Physics Laboratory and
Dept. of Mechanical Engineering,
University of Washington,
Seattle, Washington
dahl@apl.washington.edu
Phone: 206-543-2667

09 June 2014

Suggested citation:

Soloway, A.G., and P.H. Dahl. 2014. *Mine Neutralization Exercise (MINEX) Sound Measurement Trial.* Prepared for U.S. Fleet Forces Command. Submitted to Naval Facilities Engineering Command (NAVFAC) Atlantic, Norfolk, Virginia, under Contract No. N62470-10-3011, Task Order CTO 03, issued to HDR Inc., Norfolk, Virginia. Prepared by Applied Physics Laboratory and Department of Mechanical Engineering, University of Washington, Seattle, Washington. 09 June 2014.

EXECUTIVE SUMMARY

In September 2012 a team from the University of Washington, joined by personnel from Naval Facilities Engineering Command (NAVFAC) Atlantic and HDR, Inc., conducted a set of measurements of the underwater sound generated by sub-surface explosions from mine warfare exercise (MINEX) activities. In total five tests were conducted with explosive charges ranging from 0.1 to 6.0 kilograms of TNT-equivalent. The primary metrics used to quantify the sound from underwater explosions are the peak pressure generated by the explosion and the sound exposure level (SEL).

Three key findings emerged from this study:

1. The measured peak pressures were compared to the semi-empirical equation involving the scaling parameter R/W$^{1/3}$, or the range from the explosive source divided by weight to the one-third power, where P_{peak} is the peak pressure in pascals (Pa), R is the measurement range in meters, and W is the charge weight in kilograms of TNT.

$$P_{peak} = 52.4 \times 10^6 \left(\frac{R}{W^{1/3}}\right)^{-1.13}$$

   The scaling parameter is also referred to as scaled range and measurements were found to be in very good agreement with the peak pressure equation over values of scaled range going from 200 to 2,000, as expressed in meter-kilograms-sec units.

2. Using the 90 percent energy approach, the sound exposure level (SEL) for the five tests were 174–190.4 $dB\ re\ 1\mu Pa^2 s$. These results were found to be highly dependent on charge weight and range from the source, and it was determined that SEL was also well predicted using a modification of scaled range that involves an additional factor of $W^{1/3}$, which arises from a semi-empirical equation for the energy flux density. The SEL is a measure of the total acoustic energy received by an organism, and is a common metric used in environmental acoustics as it allows for the comparison of sounds of varying duration.

3. Finally, measurements of Scholte interface waves were recorded during two of the tests. The extremely low-frequency (less than 10 Hertz) Scholte wave necessitated a precise correction for the effect of resistance and capacitance in the hydrophone and receiving network. The Scholte waves arrived between 1 and $4\ s$ after the direct water arrival. Based on these arrival times, the shear speed in the sediment was estimated to be in the range of 100–370 m/s. Preliminary modeling using the wavenumber integration approach confirmed that the measured signal was a Scholte wave, and the estimate of sediment shear speed is a reasonable estimate. The Scholte wave is of relatively high amplitude for this frequency range (2-5 Hertz).

This page intentionally left blank.

TABLE OF CONTENTS

Acronyms and Abbreviations

C_s	constant value in equation for energy flux density.
$c_{scholte}$	propagation speed of Scholte wave.
c_{water}	sound speed in water
dB	decibel
E_f	energy flux density
ESD	energy spectral density
F_{90}	upper frequency below which 90 percent of the total waveform energy is contained
f	frequency
HOBO	Hobo water depth data logger
Hz	Hertz
$k_{scholte}$	Scholte wavenumber
kg	kilogram(s)
m	meter(s)
NAVFAC	Naval Facilities Engineering Command
OASES	Ocean Acoustics and Seismic Exploration Synthesis
P_{peak}	peak pressure
Pa	Pascal(s)
$p(t)$	instantaneous pressure
p_{ref}	reference pressure
rms	root-mean-square
SEL	sound exposure level
SEL_{90}	sound exposure level computed using the 90% energy approach
SEL_{100}	sound exposure level computed using the 100% energy approach
s	second(s)
T	integration period for sound exposure level
TNT	Trinitrotoluene explosive
VLA	vertical line array
W	charge weight
Z	detonation depth
Z_o	hydrostatic depth
$\lambda_{scholte}$	wavelength associated with Scholte wave
τ	bubble pulse period
ρ	material density

1. INTRODUCTION

Naval activities such as ordnance disposal, demolition and requisite training, can involve detonation of small explosive charges in shallow water. On 11 September 2012, a team from the University of Washington, along with personnel from Naval Facilities Engineering Command (NAVFAC) Atlantic, and HDR, Inc., conducted a set of measurements of the underwater sound generated by sub-surface explosions from a training exercise for a navy ordnance disposal team. The measurement site was located 7 kilometers (km) off the coast of Virginia Beach, Virginia.

This work presents these underwater sound measurements with focus on peak pressures, sound exposure levels (SEL) and time-series analysis. Additionally, the influences of elastic properties in the seabed are investigated. The goals of this work are to provide both accurate ground-truth data and improved modeling of such sound, so as to ultimately produce more accurate and precise estimates of potential impacts on marine life.

The report is organized as follows. **Section 2** presents a brief overview of underwater explosion research including semi-empirical equations for peak pressure from explosions and the calculation of the SEL. **Section 3** summarizes the Virginia Beach measurements. In **Section 4** experimental results for the peak pressure, bubble pulse period and SEL are presented. Also included here are results from the application of auditory weighting functions for marine mammals and sea turtles. In **Section 5** elastic effects are discussed and measurements of Scholte interface waves are presented. A summary is given in **Section 6**.

This page intentionally left blank.

2. BACKGROUND

Chapman [1] provided a relatively recent review and discussion of the general characteristics of underwater explosions. During the detonation of an underwater charge, the explosive material is transformed into a small sphere of gas at high temperature and pressure. As a result of the pressure differential between the gas sphere and the hydrostatic pressure in the water, a shock wave is radiated into the water. Following detonation, the gas sphere begins to expand outward resulting in a pressure tail behind the shockwave that exponentially decreases in magnitude. As the bubble expands, the pressure inside begins to decrease. When the pressure inside the bubble reaches the hydrostatic pressure of the water, the inertia of the moving gas causes the bubble to continue to expand. This continued expansion of the gas results in the pressure within the gas sphere falling below the hydrostatic pressure. Eventually the gas sphere ceases to expand. With the pressure inside the gas sphere now below the hydrostatic pressure, the bubble begins to contract thereby increasing the internal pressure. Similar to the expansion process, the inertia of the gas bubble causes the pressure within the sphere to increase past the hydrostatic pressure. This process of expansion and contraction, collectively referred to as the *bubble pulse*, continues until the energy within the gas sphere has been radiated into the water. A notional pressure history of the explosive waveform as it relates to the size of the gas sphere is shown in **Figure 1**. The time between the shock arrival, P_{peak}, and the peak pressure of the bubble pulse P_1, is referred to as the bubble pulse period, τ.

2.1 Semi-Empirical Equations

In the following section the semi-empirical equations for the peak pressure and bubble pulse delay are presented.

2.1.1 Peak Pressure

Using experimental measurements of underwater explosions collected during and after World War II, a semi-empirical equation for predicting the peak pressure from underwater explosions was developed as a function of the scaling parameter, or $R/W^{1/3}$, defined as the range from the source, R, divided by charge weight, W, to the one-third power (herein referred to as scaled range.) The term semi-empirical has been used to describe this peak pressure equation due to the origins of this parameter in Kirkwood-Bethe propagation theory [3]. The peak pressure [4] is given by

$$P_{peak} = 52.4 \times 10^6 \left(\frac{R}{W^{1/3}}\right)^{-1.13} \quad [1]$$

where $P_{peak}\ is$ the peak pressure in Pascal (Pa), R the measurement range in meters (m), and W the charge weight in kilograms of TNT (kg-TNT). It is important to note that this equation was developed for TNT, due to its historical and continued use as the standard high explosive, and assumes a spherical TNT charge of density 1520 kg/m^3 [5]. Using this equation, the peak pressure for other high explosives can be predicted through the use of TNT-equivalent weight. While originally formulated for spherical charges, the equation has been successfully employed for a wide array of charge geometries [1], [6]–[8].

While a full derivation of the Kirkwood-Bethe theory is outside the scope of this report, it has been shown [5] that the pressure in the water decays exponentially with time, and is dependent only on the explosive material and the ratio of the range to the charge radius, R/a_o. The peak-pressure equation assumes a spherical charge geometry where the charge weight is given by $W = \rho\frac{4}{3}\pi a_o^3$ where ρ denotes the density of the explosive material. With this in mind, the ratio R/a_o can be reformulated as

$$\frac{R}{a_o} = \frac{R}{W^{1/3}} \times \left(\rho\frac{4}{3}\pi\right)^{1/3} \quad [2]$$

In the peak-pressure equation $\left(\rho\frac{4}{3}\pi\right)^{1/3}$ is absorbed into the 52.4×10^6 factor. Additionally, the Kirkwood-Bethe theory supports the $R^{-1.13}$ decay of the peak pressure with range, which is a somewhat greater decay rate than the R^{-1} decay expected for spherical spreading of an acoustic wave [5].

2.1.2 Bubble Pulse Period

Following the development of the peak-pressure equations, an analogous equation for the bubble pulse period as a function of charge weight and explosion depth was developed. Specifically, this equation predicts the time delay between the arrival of the shock wave and the first bubble pulse peak. Although originally formulated using measurements of deep underwater explosions [9], this equation has previously been successfully applied to shallow charges [1]. The bubble pulse period is given by

$$\tau = 2.11 \times W^{1/3} Z_o^{-5/6} \quad [3]$$

where τ is the bubble pulse period in seconds (s) (**Figure 1**), and Z_o is the hydrostatic depth in meters (given by $Z_o = Z + 10.1\ m$). Unlike the peak pressure equation, which is a function of scaled range, the bubble pulse period is a function of charge weight and detonation depth, and should be consistent for measurements collected simultaneously at multiple ranges.

2.2 Sound Exposure Level

The SEL is the time integral of the squared acoustic pressure

$$SEL = 10\log_{10}\left(\frac{1}{p_{ref}^2}\int_0^T p^2(t)dt\right) \quad [4]$$

where SEL is in units of dB referenced to p_{ref}, which in this case is $1\ \mu Pa^2 s$. Popper [10] explained that SEL is an indication of the total acoustic energy received by an organism. It has become a useful metric to assess cumulative noise exposure as it allows for the comparison of sounds with varying durations [11].

One approach to calculating the SEL is the 90 percent energy approach (SEL_{90}). Using this approach, the integration period, T, is defined as the sample interval that includes 90 percent of the energy of the explosion's waveform. An example of this calculation is shown below (**Figure 2**). An alternate approach

is the 100 percent energy approach (SEL_{100}) where the integration window, T, includes all of the energy in the waveform.

2.3 Auditory Weighting Functions

Different classes of marine species show variable sensitivity to underwater noise based on differences in their hearing. To emphasize frequencies where sensitivity to this noise is high and de-emphasize frequencies where sensitivity is low, auditory weighting functions are used; such functions specific to the type of underwater noise studied here are from the report , "The Criteria and Thresholds for U.S. Navy Acoustic and Explosive Effects Analysis" [12].

In Finneran et al. [12], six functional hearing groups are identified (**Table 1**), one for turtles, and five for marine mammals with all species in a specific group considered to be equally susceptible to noise. The auditory frequency ranges listed in **Table 1** should not be confused with auditory weighting functions, as the former serve merely as a guide to the range of auditory reception. Auditory weighting functions derived from the equations in Finneran et al. [12] corresponding to the six functional hearing groups are shown in **Figure 3**, and their interpretation is as follows: Energy at frequencies for which the weighting is less than 0 dB is discounted or given less weight in an energy metric such as the SEL (e.g., the auditory weighing function associated with Phocids and Sirenians calls for such a reduction for frequencies less than about 100 Hertz [Hz]). Additional details on the creation and interpretation of auditory weighting function pertaining to the effects of underwater sound on marine life can be found in Southall et al. [11].

2.4 Elastic Parameters in the Sediment

Scholte waves are a type of seismic wave that propagates along the water-seabed interface at a speed equal to approximately 90–95 percent of the speed associated with propagation of shear waves in an elastic medium [13]. The Scholte wave propagates parallel to the seabed and causes a rolling motion in the sediment (**Figure 4[a]**), while perpendicular to the seabed it decays exponentially with distance away from the interface in both the water and the sediment.

At the water-sediment interface, the Scholte wave has retrograde elliptical particle motion (**Figure 4[b]**). With increasing depth into the sediment the horizontal component decreases until the particle velocity becomes purely vertical at a distance of approximately one-fifth of the wavelength associated with Scholte wave propagation in the sediment given by

$$\lambda_{scholte} = \frac{2\pi}{k_{scholte}} \qquad [5]$$

Where the Scholte wavenumber $k_{scholte}$ is given by

$$k_{scholte} = 2\pi f \left(\frac{1}{c_{water}^2} - \frac{1}{c_{scholte}^2} \right)^{1/2} \qquad [6]$$

with c_{water} being the sound speed in the water, and $c_{scholte}$ speed of propagation of the Scholte wave. At greater depths the particle motion once again becomes elliptical albeit with pro-grade motion[13]. Additionally, the amplitude of the Scholte wave decays to zero within one wavelength from the water-sediment interface. As result , lower frequencies (with larger wavelengths) penetrate deeper into the sediment [14].

Another important feature is the frequency dependence of the Scholte wave speed, or dispersion. For a homogeneous medium the Scholte wave is non-dispersive, however real environments typically have complex bottoms with layers, and shear and compressional speed gradients that increase with depth. For these environments the Scholte wave is dispersive with low frequencies arriving first, followed by the higher frequencies. The dispersive properties of the Scholte wave can be understood qualitatively since lower frequencies have greater penetration depth into the seabed and the shear and compressional speed increases with depth. Lower frequencies will excite deeper layers with higher shear and compressional speeds, and as a result will arrive at an earlier time.

Previous studies of Scholte wave propagation in sandy bottoms have shown the frequency content of Scholte waves to be in the range of 1–30 Hz and group speeds in the order of 100–400 m/s [15]–[18]. As these group speeds are well below the speed of sound in the water, the Scholte wave arrival follows that of the direct water arrival.

Studies have shown that the excitation of Scholte waves can be difficult, even when the experiment has been specifically tailored to that goal [15]. First, the source (the explosive charges in the case of this report) must be within one wavelength of the ocean bottom or else the Scholte wave will not be excited. Additionally, as there is strong attenuation of Scholte waves in ocean bottoms where the shear speed is less than the speed of sound in the water [16], a strong enough source is required to sufficiently excite the Scholte wave.

3. VIRGINIA BEACH MINEX TRIAL

3.1 Measurement Site

The underwater explosion measurements were conducted on 11 September 2012 at a site located approximately 7 km off the coast of Virginia Beach, Virginia. The measurement site encompasses four locations; the MINEX detonation site, and the mooring locations of the two measurement vessels involved, as discussed below, one of which was placed in two mooring positions over the course of the day (**Figure 5**). For purposes of this report, this area can be considered a rectangle of dimension 950 × 200 m that includes all four locations in **Figure 5**.

Based on existing bathymetric data from the National Oceanic and Atmospheric Administration, the mean lower low water depth of 14.3 m, where mean lower low water is defined as the average of the lower low water height of each tidal day observed over the National Tidal Datum Epoch. Tidal data for the measurement site were estimated using data from the Chesapeake Bay Bridge Tunnel tidal station (located at 36 43.2, N 76 06.84 W, 27 km from the measurement site), obtained from the National Oceanic and Atmospheric Administration Center for Operational Oceanographic Products and Services. Owing to tidal variations throughout the day (**Figure 6**), the actual water depth during the experiment varied between 14.7 and 15.0m.

Studies in the vicinity of the measurement site, conducted by the Virginia Institute of Marine Science to determine the feasibility of sand mining [20]–[23], provided data on the seafloor. Data from bottom grabs and core samples from these studies show a seabed composed of unconsolidated sediments consisting of fine to course sand and clay, with significant spatial variation (**Figure 7**).

Profiles of sound speed versus depth in the water column were recorded using a YSI Castaway CTD device, which computes the sound-speed profile from direct measurements of temperature, conductivity (surrogate for salinity), and water depth. Sound-speed profiles were sampled at two times, 8:41:31 and 11:24:23 local time (**Figure 8**), and were found to be approximately iso-speed at 1528 m/s. Owing to significant heave motion experienced by the two research vessels we did not allow this instrument to strike the seabed and risk damage, hence the CTD measurements do not extend to the bottom. This should not be considered an issue as the sound speed varies little with depth particularly in the vicinity of the seabed.

During the experiment there existed a swell- wave field originating from the Northeast that was not linked with local wind conditions. Sea surface wave data was obtained from the National Data Buoy Center's (NDBC) Cape Henry 44099 wave buoy located at 36 54.9 N, 75 43.2 W, 19 km Northeast from the test site. During the measurement period significant wave height, defined as four times the root mean square (rms) of the wave height, varied between 1.0 m and 1.2 m; alternatively the rms wave height varied between 0.25 and 0.3 m.

3.2 Test Description

Five explosive charges were deployed as part of the Navy explosive ordnance disposal team's training exercise (**Table 2**). These charges had TNT equivalent weights ranging from 0.1–6.0 kg. The detonations occurred at either (approximately) 9 m depth, or on the bottom. Tests 1–4 used C-4 charges with a TNT-equivalence of 1.34 (i.e., 1 kg of C-4 produces an explosive force equivalent to 1.34 kg of TNT), while Test 5 used a CH-6 charge with a TNT-equivalence factor of 1.5.

3.3 Equipment and Measurement Locations

Measurements were made from two Vessels; the R/V *Ocean Explorer* (Vessel 1) located 430 m from the underwater detonation site for Tests 1–5 and the F/V *Instigator* (Vessel 2) located 165 m away for Tests 1–2 and 950 m away for Tests 3–5 (**Figure 5**).

From Vessel 1, acoustic data were recorded using a vertical line array (VLA), and an autonomous recording device (Loggerhead Instruments DSG) (**Figure 7**). The VLA elements consisted of nine hydrophones (ITC 1032) with 0.7 m spacing. Data from the VLA were recorded on a multi-channel coherent data acquisition system (Astro-Med DASH-20) with each channel sampled at 62,500 Hz sampling frequency. The autonomous system consisted of a single hydrophone recording at a sampling frequency of 50,000 Hz. The VLA and autonomous system were attached to a weighted line secured to a davit. A HOBO data logger (HOBO), used to measure water depth, was also attached to the line and was mounted exactly halfway between Hydrophones 2 and 3. The hydrophone depths of the VLA and autonomous system were determined using these depth measurements. A summary of the hydrophone depths can be found in **Table 3**.

From Vessel 2, acoustic data were also recorded using the same autonomous system system as Vessel 1. Similar to the Vessel 1 setup, this system was attached to a boat-mounted line (**Figure 9**), and a HOBO data logger was used to determine the hydrophone depths (summarized in **Table 3**).

4. RESULTS AND DISCUSSION

Results and brief discussion relating to the energy spectral density (ESD) (**Section 4.1**), peak pressure and bubble pulse delay measurements with comparisons to predicted values (**Section 4.2**), and SEL_{90} (**Section 4.3**) for all five tests are presented. The application of the U.S. Navy auditory weighting functions [12] to the ESD is also presented (**Section 4.4**). Finally, **Section 4.5** gives preliminary results and discussion concerning the observation of Scholte waves in the data, the role of sediment elasticity in the generation of such waves, and related preliminary estimates of elastic parameters in the sediment. Tabulated data for this section can be found in **Appendices A and B**.

4.1 Energy Spectral Density and Third Octave Band Levels

Given the transient nature of the explosion pressure signal, the spectral content of the signal is appropriately conveyed by an Energy Spectral Density (ESD). **Figure 10** shows the ESD for the five tests measured from Vessel 1 (Hydrophone 1 of the VLA) and **Figure 11** shows the ESD simultaneously measured from Vessel 2. For each ESD, a narrow band estimate for which the frequency resolution (Δf) equals 1 Hz and third-octave spectral smoothing estimate is shown.

It is readily seen that the majority of the energy is contained in the low-frequency range, approximately between 100 and 1,000 Hz. Spectral interference lines revealed in the narrow band estimates (blue lines) are related to the time interference of the bubble pulses, and the overall ESD levels are highly dependent on explosive charge weight and measurement range [24], [25].

The upper frequency below which 90 percent of the total waveform energy is contained, identified as F_{90}, has been calculated for Tests 1–5 (Table 4) at the request of NAVFAC-LANT. The resulting F_{90} values are also found to be highly dependent on charge weight with F_{90} decreasing with increasing charge weight.

4.2 Comparison of Measurements to Semi-Empirical Equations

4.2.1 Peak Pressure

The peak pressure data recorded at Vessel 1 are shown with respect to depth in **Figure 12**, and show only weak variation with depth. Additionally, the Loggerhead and VLA data are in good agreement. Due to the weak depth variation, in this section the peak pressures for Vessel 1 will be presented as a single value averaged across the 9 VLA hydrophones

The peak pressures from the Vessel 1 and Vessel 2 measurements and the levels predicted by Equation 1 are plotted with respect to scaled range in **Figure 13**. A comparison of the measured and predicted levels shows reasonable agreement for the scaled-range parameter values that go from approximately 250 to 2,000 $m\ kg^{-1/3}$. Note that there exists uncertainty in source-receiver distances for each test owing to uncertainty in vessel mooring location obtained from GPS data, and mooring watch circles that were in effect, and a nominal uncertainty of $\pm 50\ m$ is estimated. From the peak pressure equation, this ± 50 m uncertainty translates to $\pm 1\ dB$ at the 430-m and 950-m measurement ranges, and increases to $\pm 5\ dB$ for the 165-m range.

To better illustrate how the measured data compare to predictions from Equation 1, results from Virginia Beach have been plotted against predicted levels along with experimental results from previous

studies by Arons [4], Cole [26], and Murata et al. [7] (**Figure 14**). While the measurements from previous studies correspond to varying charge weights, explosive materials, and measurement ranges, there is good agreement between results from the various studies and the levels predicted by the peak pressure equation.

A final point of interest in the study of the peak pressure is the effect of detonation depth on the peak pressure. In **Figure 15** the peak pressure measurements have been identified by their appropriate detonation depth (9 m or bottom). Bottom charges typically fall at or below the predicted values, while the 9-m charges are typically at or above the predicted levels.

4.2.2 Bubble Pulse Delay

The bubble pulse delay was determined from the auto-correlation of the measurement time series, where the bubble pulse delay was the time between the first and second peak values of the auto-correlation function. The measured and predicted bubble pulse periods (from Equation 3) are compared in **Table 5**. The comparative results for the C-4 charges (Tests 1–4) indicate good agreement between the measured and predicted bubble pulse period values, with measured values always lower than predicted values. The measured bubble pulse period value for the CH-6 charge (Test 5), however, varies considerably from predictions with a much longer bubble pulse period.

The bubble pulse delay period has been used in previous studies to estimate the detonation depth for a given charge of known weight [27] using Equation 3. Applying this approach to our data we found general agreement for Tests 1-4 (**Table 2**) insofar as calculated depths based on the bubble pulse period were reasonably consistent with the nominal detonation depths provided by the navy (despite calculations for Tests 2 and 3 yielding values slightly greater than the water depth). A notable exception is Test 5 where the calculated depth (2.5 m) differs significantly from the 9-m nominal depth.

4.3 Sound Exposure Level

Using the SEL_{90} results from the VLA and Loggerhead at 430 m, the SEL_{90} values vary only weakly with depth, and the VLA and Loggerhead measurements are in good agreement (**Figure 16**). Given the weak depth variation, the SEL for Vessel 1 will be shown as a single value averaged across the 9 VLA hydrophones in the remainder of the results in this section. Tabulated results for SEL_{90} can be found in **Appendix A**, along with additional results for SEL_{100}.

The SEL_{90} values recorded from Vessels 1 and 2 are shown in **Figure 17** plotted against scaled range. Unlike the peak pressure, which is dependent only on the scaled range parameter, explosive charges of different weight but at the same scaled range value can result in different SEL_{90}, with the larger charges exhibiting higher SEL_{90} levels. Our data provides only limited evidence of this, for example, as best exhibited by the two estimates made at a scaled range of approximately $500\ m/kg^{1/3}$ that differ by at least 5 dB.

Upon further investigation of the technical literature we found an alternate scaling approach from the calculation of the energy flux density E_f [7] given by

$$E_f = C_s\, W^{1/3} \left(\frac{W^{1/3}}{R} \right)^{2.12} \qquad [7]$$

where C_s is a constant. Given that SEL is a measure of the sound energy, SEL_{90} was plotted against $W^{1/3}\left(W^{1/3}/R\right)^{2.12}$ to determine if a simple equation for predicting SEL can be developed (**Figure 18**). Using this alternate scaling approach, the SEL_{90} data collapse onto a single line and exhibits a linear trend when expressed in decibels. This shows promise for the development of an empirical equation for SEL. Importantly, we anticipate that the relationship for SEL with E_f-based range scaling from Equation 7 as just described can be adapted to weighted measures of SEL, such as sea turtle and marine mammal weighting. Weighted measures are discussed further in **Section 4.4**.

4.4 Application of Auditory Weighting Function

The auditory weighting functions for the functional hearing groups have been applied to the ESD for the Test 4 measurements recorded from Vessel 1 on hydrophone 1 of the VLA (**Figure 19**). As noted in **Section 2.3**, the auditory weighting functions emphasize ESD levels where hearing sensitivity is expected to be high, and reduces the levels where hearing sensitivity is expected to be low.

SEL are also calculated for the weighted data (see tabular results in **Appendix B**). While the resulting levels are highly dependent on the functional hearing group, it should be readily apparent that weighted SEL will always be less than un-weighted SEL.

While we cannot comment on the protective efficacy of auditory weighting functions we do note that their application can modify the zone of influence for a particular marine species. For example, weighted SEL for mid- and high-frequency cetaceans is expected to have a higher transmission loss than un-weighted SEL (particularly in deep water) owing to the emphasis of higher frequency content and de-emphasis of lower frequency content, and thus the zone of influence will be reduced as a result of weighting.

4.5 Elastic Parameters in the Sediment

In shallow water (where there is significant interaction of sound with the water surface and ocean bottom), very low frequencies (below 50 Hz) often do not make significant contributions to the sound field. However, during the 2012 Virginia Beach measurements very low frequency measurements of order O(1–10 Hz) from Scholte waves traveling along the water-sediment interface were recorded from Vessel 1 on the VLA.

4.5.1 Scholte Wave Time History and the Shear Speed in the Sediment

Measurements of Scholte waves were discovered in the Test 3 and Test 4 data recorded from Vessel 1 on the VLA. Time histories of the Scholte wave show arrival times between $1\ s$ and $4\ s$ after the direct water arrival (**Figures 20 and 21**). Using measurements of the water sound speed (1,528 m/s), the range of Vessel 1 (430 m), and knowing that the Scholte wave velocity is typically 90% of the shear speed, the shear speed in the sediment was estimated to be in the range of 100–370 m/s. These values are in good agreement with Hamilton's results for the shear wave velocity in sand and clay [28].

At this point the question arises as to why Scholte waves were recorded in Tests 3 and 4 but not in the other three tests. While it is difficult to give a conclusive answer to this, the likely reasons are tied to the charge weights. Tests 3 and 4 (TNT-equivalent weight 3 kilograms [kg] and 6 kg respectively) represent

the largest charges used. As the Scholte wave experiences high attenuation rate in sand and clay sediment, these larger charges were likely able to provide sufficient energy to generate a propagating Scholte wave while the smaller charges could not.

4.5.2 Energy Spectral Density of Scholte Waves

Most of the energy carried by the Scholte wave was in the very low-frequency range between 1 and 10 Hz for both tests (**Figures 22 and 23**). Additionally, the deeper hydrophones (those closer to the water-sediment interface) typically measured higher levels than the more shallow hydrophones. As an example, the Test 4 ESD levels, between 1 and 6 Hz, for hydrophone 1 (nominal depth of 12.2 m) were consistently higher than levels from hydrophone 9 (nominal depth of 6.6 m). As the amplitude of the Scholte wave should decay exponentially away from the water-sediment interface, these results are expected. While the ESDs for the two tests showed some similarities, the ESD levels for Test 3 were typically lower than the Test 4 levels. Additionally, the ESD for Test 3 peaked at 4.5 Hz while Test 4 had a peak value at 3.5 Hz.

4.5.3 Time-Frequency Analysis

Time-frequency analysis of the Scholte wave data revealed dispersive characteristics, with lower frequencies (approximately 2 Hz) arriving followed by higher frequencies (approximately 5 Hz) (**Figures 24 and 25**). The trend of the dispersive effects was similar for Tests 3 and 4. Interface waves in a homogenous seabed are non-dispersive [14]. Thus this dispersion reveals characteristics indicative of a complex seabed, which may include features such as layering, a sound-speed gradient, and additional attenuation due to shear. The characteristics of the dispersion are in good agreement with results from previous studies [15]–[18].

4.5.4 Wavenumber Integration Modeling

To verify that the waveforms measured in Tests 3 and 4 are Scholte waves, preliminary modeling was done using the Ocean Acoustics and Seismic Exploration Synthesis (OASES) computer code for modeling seismo-acoustic propagation using wavenumber integration and the Direct Global Matrix Approach [29]. Using OASES, three geo-acoustic models were used; a layered bottom that does not support shear, a single layered homogeneous bottom with constant shear speed, and a shear-supporting layered bottom. It should be noted that the purpose of this modeling was to investigate the effects of a layered bottom on the Scholte wave, and all results are preliminary at this stage. Nevertheless, the preliminary modeling results are in good agreement with our measurements insofar as they predict the observed dispersive effect.

Note that a layered bottom that does not support shear (**Figure 26**) only shows the water arrival at 0.4 s. As shear is not supported in this model, a later arrival resulting from shear in the sediment would not be expected. For the single layered homogeneous bottom with constant shear speed (**Figure 27**), the water arrival is once again visible. An additional arrival, the Scholte wave, at approximately 2 s can also be seen. As expected, this later arrival does not exhibit dispersion characteristics. Finally in the results for a shear-supporting layered bottom (**Figure 28**) water arrival at 0.4 s once again is present, with an additional waveform (the Scholte wave) arriving between 1.5 and 2.5 s. Unlike the Scholte wave for the homogeneous shear-supporting bottom, the characteristic Scholte wave dispersion is present in the shear-supporting, layered bottom results. These results are similar to the Scholte waves measured in Tests 3 and 4.

5. SUMMARY

In September 2012 a team from the University of Washington, joined by personnel from NAVFAC Atlantic and HDR Environmental, conducted a set of measurements of the underwater sound generated by sub-surface explosions as part of a naval training exercise. Five test charges, ranging in weight from 0.1 to 6 kg-TNT, were deployed. Measurements were collected at distances from the testing location: 165 m, 430 m, and 950 m. Acoustic data were recorded at 430 m using a vertical hydrophone array attached to a DASH20 data recorder for all five tests, and using single-element autonomous Loggerhead systems at 165 m for Tests 1 and 2 and 950 m for Tests 3-5.

Measured peak pressures and bubble pulse delays were compared to semi-empirical equations of scaled range and are in good agreement for scaled ranges 250 to 650 $m\ kg^{-1/3}$. For scaled ranges from 650 to 2,000 $m\ kg^{-1/3}$ measured results varied up to 3 dB from predicted levels. Overall, the measurements and predicted peak pressures were in good agreement. The bubble pulse periods for the C-4 charges (Tests 1-4) were in good agreement with the semi-empirical equation. The bubble pulse period for the CH-6 charge (Test 5), however, varied significantly from the prediction.

The measured SEL_{90} ranged from 174.0 to 190.4 $dB\ re\ 1\mu Pa^2 s$. Unlike the peak pressure equation, various charge weights with the same scaled range did not result in the same levels. For two charges with the same scaled range, the larger charge generated a higher SEL. Plotting the SEL_{90} using an alternate scaling approach borrowed from the empirical equation for the energy flux spectrum, however, shows promise for the development of an empirical equation for *SEL*.

Measurements of Scholte interface waves were recorded during Tests 3 and 4. The Scholte waves had arrival times between 1 and 4 s after the direct water arrival, and were of very low frequencies on the order of 1–10 Hz. Based on these arrivals, the shear speed in the sediment was estimated to be in the range of 100–370 m/s. These estimates have been confirmed through preliminary modeling using the wavenumber integration approach. Additionally, time-frequency analysis of the Scholte waves revealed dispersive characteristics, where low frequencies arrive first followed later by higher frequencies.

The following are recommended key areas for further research that would have direct benefit to the navy:

1. Further study on how the proximity of explosive detonation to the seabed floor, as distinct from water column, influences the peak pressure (and thus predictions peak pressure based scaled range parameter), the bubble pulse time delay (and thus predictions of explosion depth), and the generation of Scholte waves.
2. Further investigation on use of the scaling from energy flux density to develop an improved empirical equation for SEL prediction and weighted SEL prediction for use by NAVFAC and other regulatory agencies.
3. Continued investigation of Scholte waves generated by underwater explosions, and how they can be utilized to improve geo-acoustic models for a given measurement site, and thereby improve underwater sound propagation modeling.
4. Future measurements should include geophone and/or vector sensor measurements to obtain measure of acoustic particle velocity in underwater explosions.

5. Future measurements should include a portable wave buoy to investigate the effects of a rough sea surface on sound propagation.

6. REFERENCES

[1] N. R. Chapman, “Measurement of the waveform parameters of shallow explosive charges,” *J. Acoust. Soc. Am.*, vol. 78, no. 2, pp. 672–681, Aug. 1985.

[2] J. B. Gaspin, J. A. Goertner, and I. M. Blatstein, “The determination of acoustic source levels for shallow underwater explosions,” *J. Acoust. Soc. Am.*, vol. 66, no. 5, pp. 1453–1462, 1979.

[3] J. G. Kirkwood and W. W. Wood, *Shock and detonation waves*. New York: Gordon and Breach, 1968.

[4] A. B. Arons, “Underwater Explosion Shock Wave Parameters at Large Distances from the Charge,” *J. Acoust. Soc. Am.*, vol. 26, no. 3, pp. 343–346, 1954.

[5] R. H. Cole, *Underwater explosions.* Princeton: Princeton Univ. Press, 1948.

[6] J. Wakeley, “Pressure-signature model for an underwater explosive charge,” *U.S. Navy journal of Underwater Acoustics*, vol. 27, no. 2, pp. 445–449, 1977.

[7] K. Murata, K. Takahashi, and Y. Kato, “Measurements of Underwater Explosion Performances by Pressure Guage Using Fluoropolymer,” *J. Mater. Process. Technol.*, vol. 85, no. 1–3, pp. 0924–0136, 2002.

[8] M. E. dos Santos, M. N. Couchinho, A. R. Luis, and E. J. Goncalves, “Monitoring underwater explosions in the habitat of resident bottlenose dolphins,” *J. Acoust. Soc. Am.*, vol. 128, no. 6, pp. 3805–3808, 2010.

[9] J. F. Slifko, “Pressure-Pulse Characteristics of Deep Explosions as Functions of Depth and Range,” United States Naval Ordnance Laboratory, NOLTR 67-87, 1967.

[10] A. N. Popper and M. C. Hastings, “The effects of anthropogenic sources of sound on fishes,” *J. Fish Biol.*, vol. 75, no. 3, pp. 455–489, Aug. 2009.

[11] B. L. Southall et al. “Marine mammal noise exposure criteria: Initial scientific recommendations.,” *J. Acoust. Soc. Am.*, vol. 125, no. 4, pp. 2517–2517, Apr. 2009.

[12] J. J. Finneran, A. K. Jenkins, and S. S. C. Pacific, “Criteria and thresholds for US Navy acoustic and explosive effects analysis,” *SPAWAR Mar. Mammal Program San Diego Calif.*, 2012.

[13] T. Lay and T. C. Wallace, *Modern global seismology*. San Diego: Academic Press, 1995.

[14] D. Rauch, “Seismic Interface Waves in Coastal Waters: A Review,” SACLANTCEN, La-Spezia, Italy, SR-42, Nov. 1980.

[15] W. A. Kuperman and F. B. Jensen, Eds., *Bottom-interacting ocean acoustics*. New York: Published in cooperation with NATO Scientific Affairs Division by Plenum Press, 1980.

[16] T. Akal, J. M. Berkson, SACLANT ASW Research Center, and Symposium on Ocean Seismo-Acoustics, Eds., *Ocean seismo-acoustics: low-frequency underwater acoustics*. New York: Published in cooperation with NATO Scientific Affairs Division [by] Plenum Press, 1986.

[17] S. E. Dosso, "Measurement of seismo-acoustic ocean-bottom properties in the high Arctic," *J. Acoust. Soc. Am.*, vol. 98, no. 3, p. 1657, 1995.

[18] G. Nolet and L. M. Dorman, "Waveform Analysis of Scholte Modes In Ocean Sediment Layers," *Geophys. J. Int.*, vol. 125, no. 2, pp. 385–396, 1996.

[19] P. M. Shearer, *Introduction to seismology*. Cambridge; New York: Cambridge University Press, 1999.

[20] C.H. Hobbs III, "Investigations of isolated sand shoals and associated deposits Virginia inner shelf," Virginia Institute of Marine Science, College of William and Mary, Gloucester Point, Virginia, Final Contract Report, Mar. 1996.

[21] S. M. Kimball and J. K. Dame, "Geotechnical evaluation of sand resources on the inner shelf of southern Virginia: Report & Appendices A-B," College of William and Mary School of Marine Science, Virginia Institute of Marine Science, Virginia Beach, Virginia, Final Report, Aug. 1989.

[22] C. Hobbs III, "Sediments and shallow stratigraphy of a portion of the continental shelf of southeastern Virginia."

[23] C.S. Hardaway, C.H. Hobbs III, and D.A. Milligan, "Investigations of Offshore Beach Sands: Virgninia Beach and Sandbridge, Virginia," Virginia Institute of Marine Science, College of William and MAry, Gloucester Point, Virginia, Oct. 1995.

[24] D. E. Weston, "Underwater Explosions as Acoustic Sources," *Proc. Phys. Soc.*, vol. 76, no. 2, p. 233, Aug. 1960.

[25] A. C. Kibblewhite and R. N. Denham, "Measurements of Acoustic Energy from Underwater Explosions," *J. Acoust. Soc. Am.*, vol. 48, no. 1B, pp. 346–351, 1970.

[26] S. Temkin, "A Review of the Propagation of Pressure Pulses Produced by Small Underwater Explosive Charges.," Rutgers University, New Brunswick, NJ, Memorandum NRL-MR-6181, 1988.

[27] N. R. Chapman, "Source levels of shallow explosive charges," *J. Acoust. Soc. Am.*, vol. 84, no. 2, pp. 697–702, 1988.

[28] E. L. Hamilton, "Elastic properties of marine sediments," *J. Geophys. Res.*, vol. 76, no. 2, pp. 579–604, 1971.

[29] H. Schmidt, *Ocean Acoustics and Seismic Exploration Synthesis (OASES)*. Department of Ocean Engineering Massachusettes Institute of Technology, 2012.

7. ACKNOWLEDGMENTS

Funding and project management support for this study was provided by US Fleet Forces Command and NAVFAC Atlantic. The authors would also like to acknowledge Anurag Kumar (NAVFAC Atlantic) for initiating this study, Daniel Engelhaupt (HDR) for logistical help and vessel arrangements, Sarah Rider and Cara Hotchkin (NAVFAC Atlantic) for providing meta data associated with the MINEX trial, Brian Amrhein (U.S. Navy EOD Instructor) for providing data concerning the test charges, the US Navy EOD team, and David Dall'Osto and Dara Farrell (University of Washington) for their valuable assistance in the field.

This page intentionally left blank.

8. FIGURES

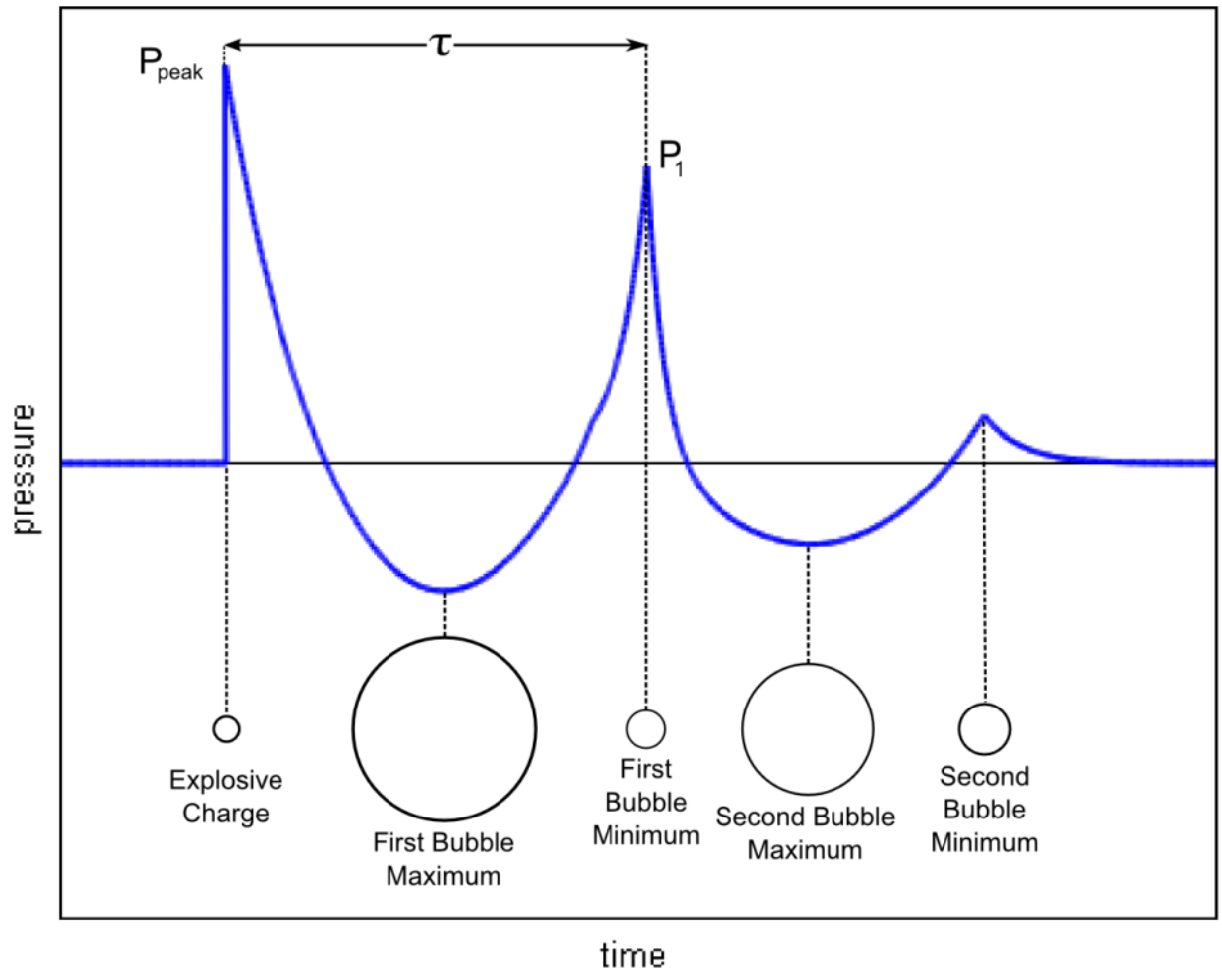

Figure 1: Notional pressure-time history for an underwater explosion with the size of the gas sphere is shown in relation to the explosion waveform [2].

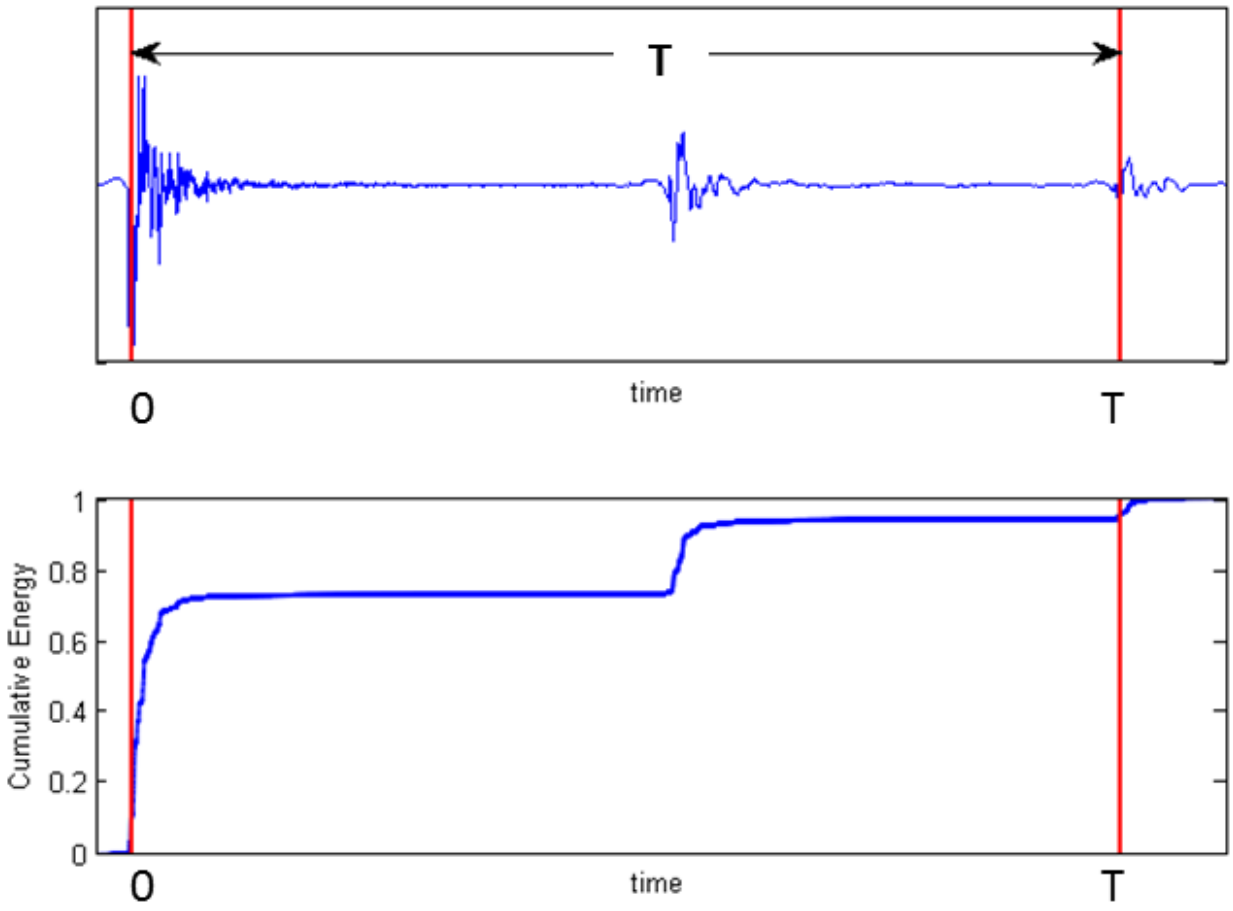

Figure 2: a) Time history of an explosion and b) the resulting time history of its cumulative energy. Red lines indicated the start and end times of the window containing 90 percent of the waveform energy.

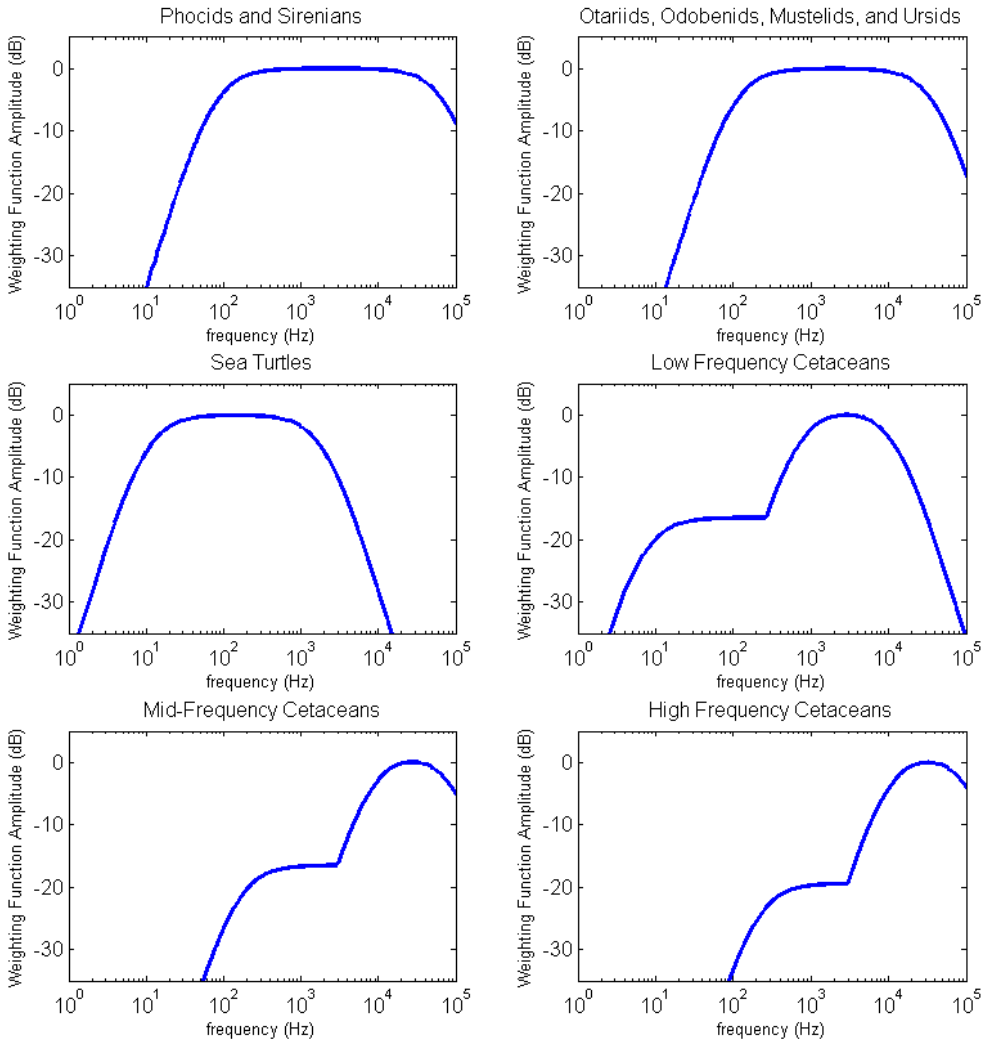

Figure 3: Auditory weighting functions corresponding to the 6 functional hearing groups (Table 1).

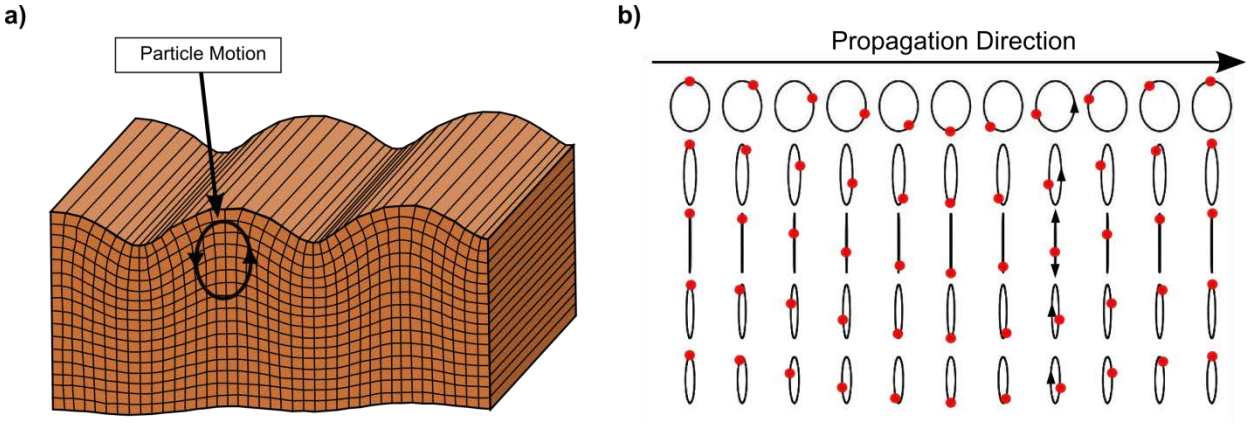

Figure 4: a) Surface wave displacement resulting from Scholte wave propagation and b) Particle motion of Scholte wave in sediment [19].

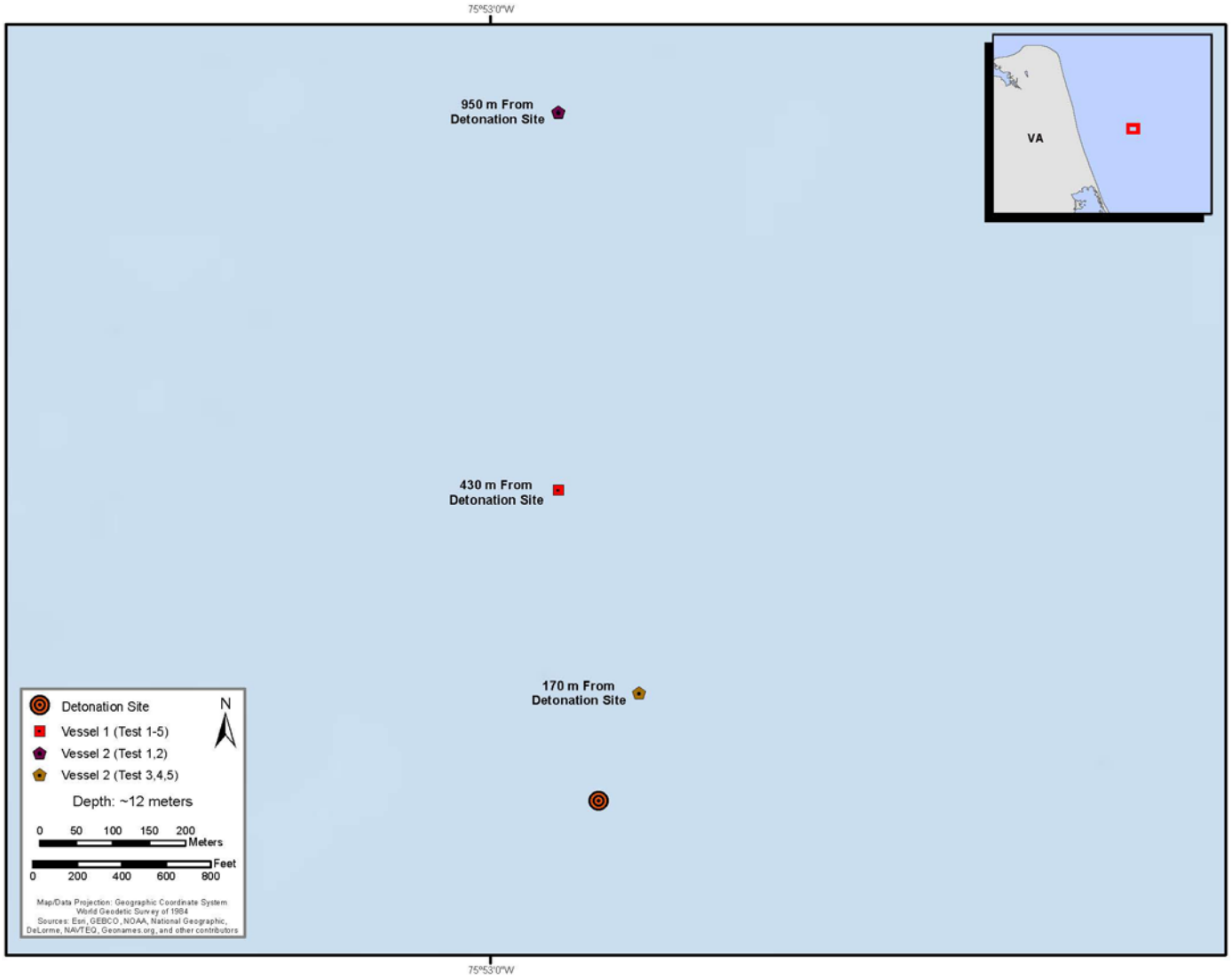

Figure 5: Map of measurement site with the locations of Vessel 1, Vessel 2, and the detonation site. The measurement site and wave buoy location in relation to the Virginia coastline can be found in the inset map.

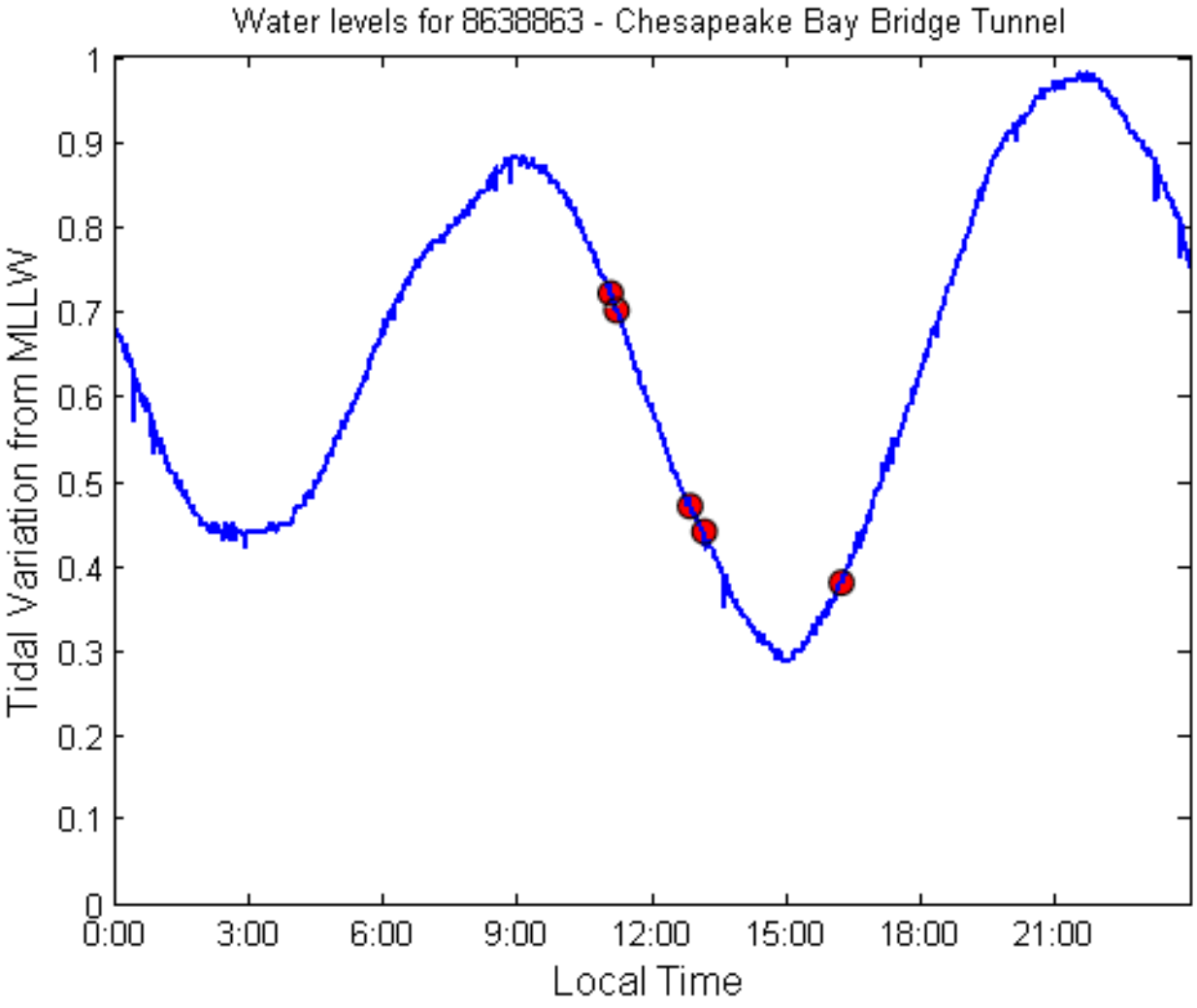

Figure 6: Tidal variation from Chesapeake Bay Bridge Tunnel tidal station. Height is the tidal variation from the meters mean low lower water in meters. Red markers indicate underwater detonation times.

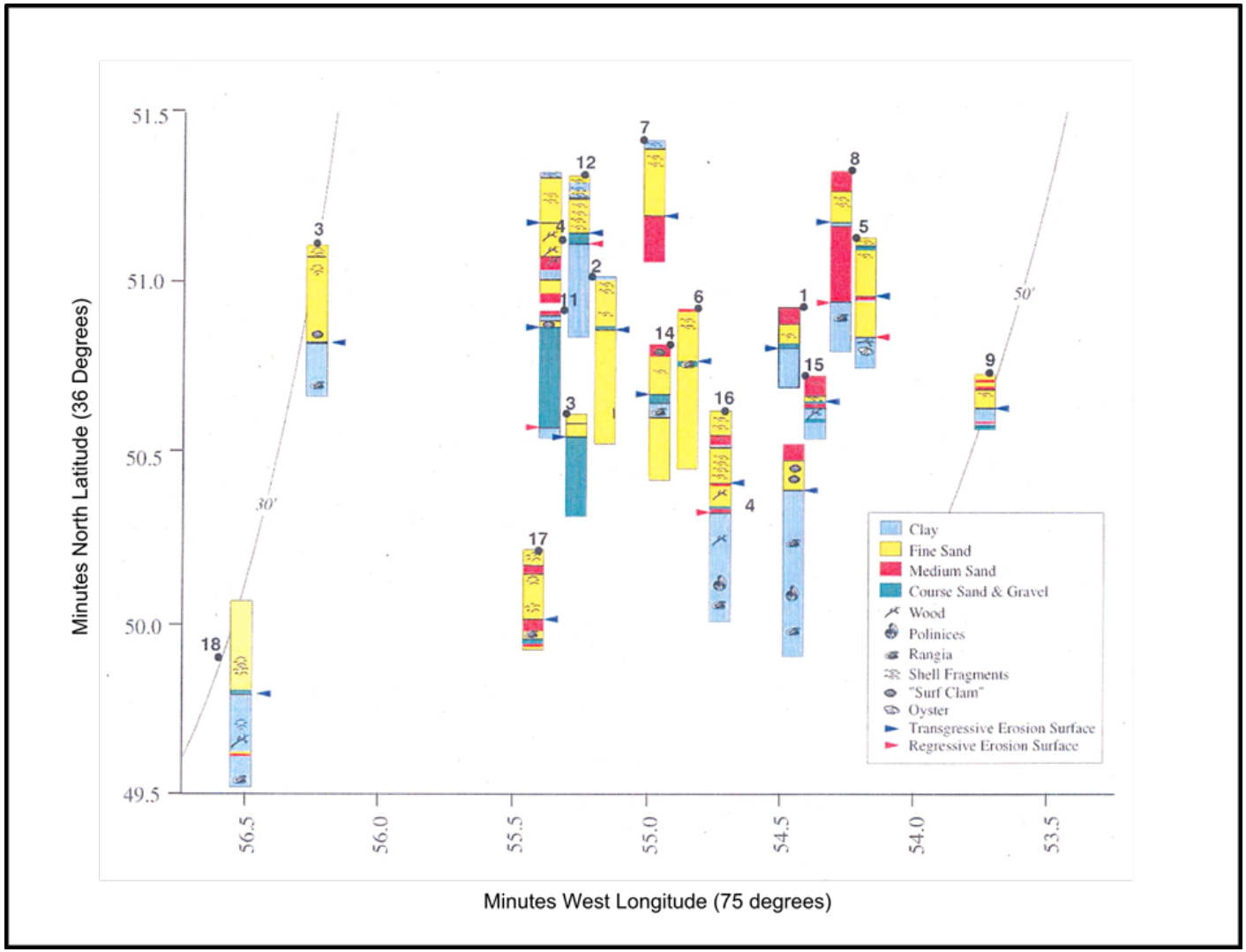

Figure 7: Schematic showing core samples taken from a site located 1.6 km Northwest of the measurement site. This schematic shows the composition of 18 bottom core samples (numbered 1–18 in the original report), along with 30 ft and 50 ft water depth contours. Additional information on the core samples can be found in the original report. [23].

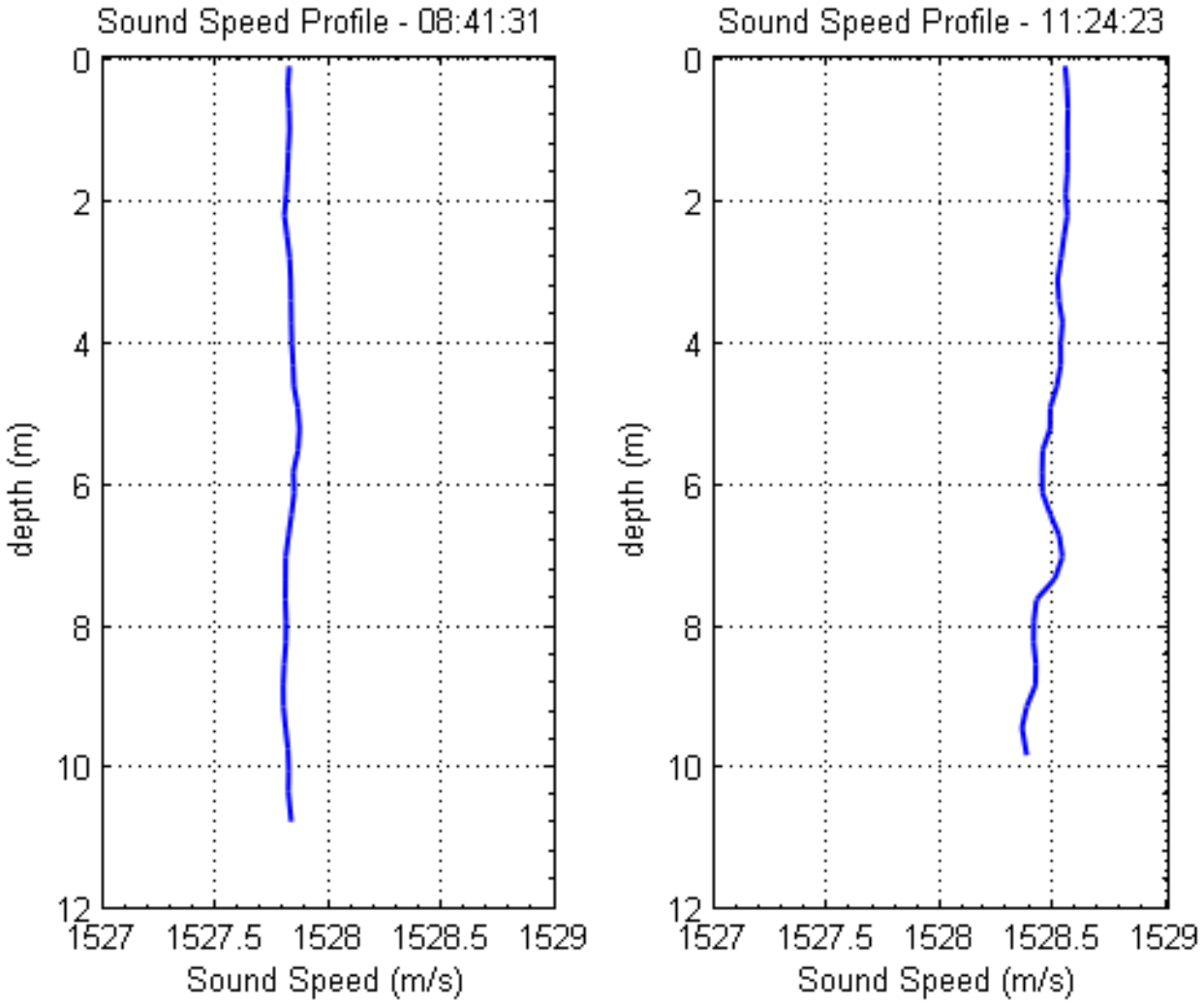

Figure 8: Sound-speed profiles collected using YSI CastAway CTD device at the corresponding collection times.

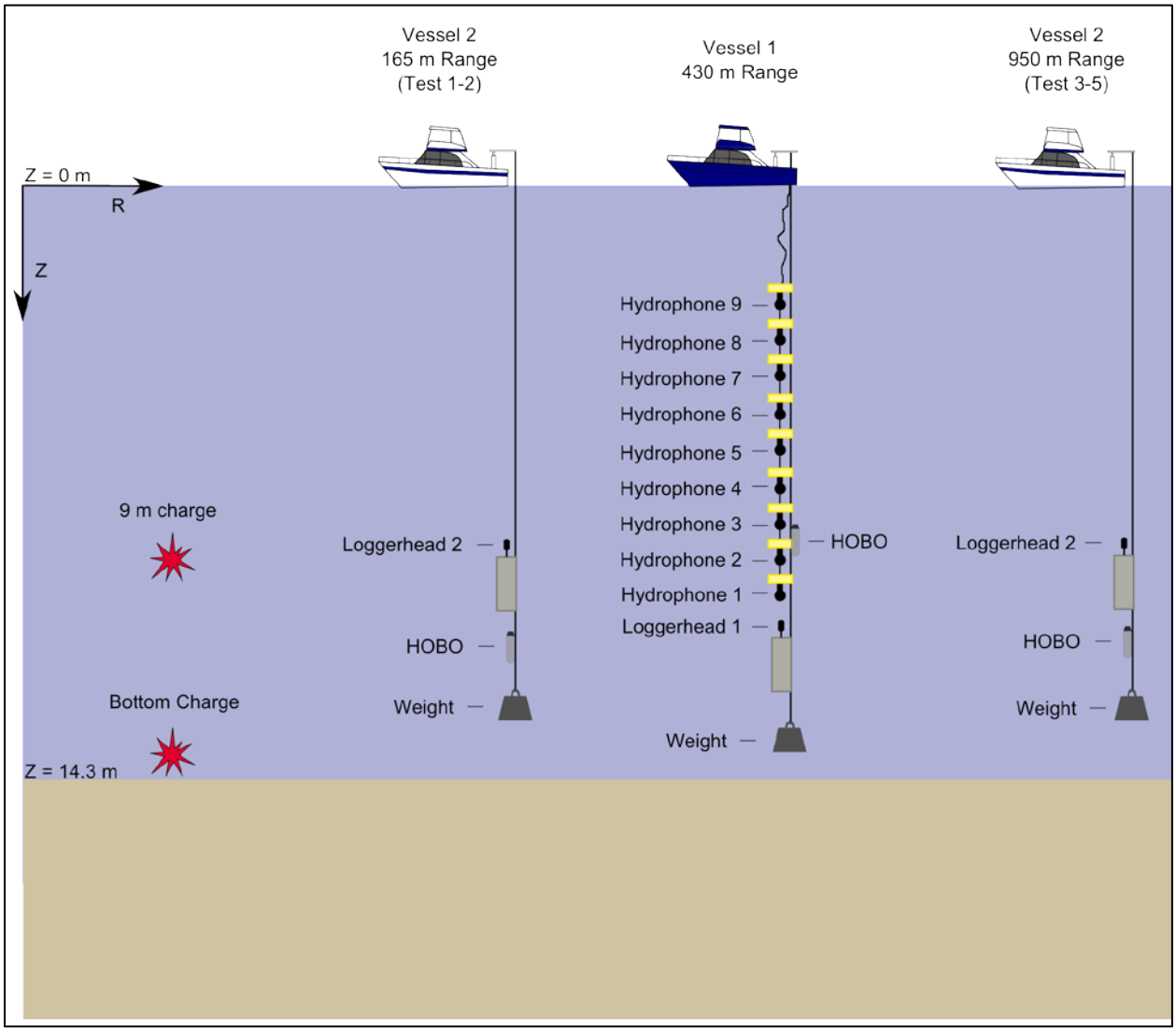

Figure 9: Experiment geometry for the Virginia Beach MINEX trial. Equipment depths are listed in Table 3.

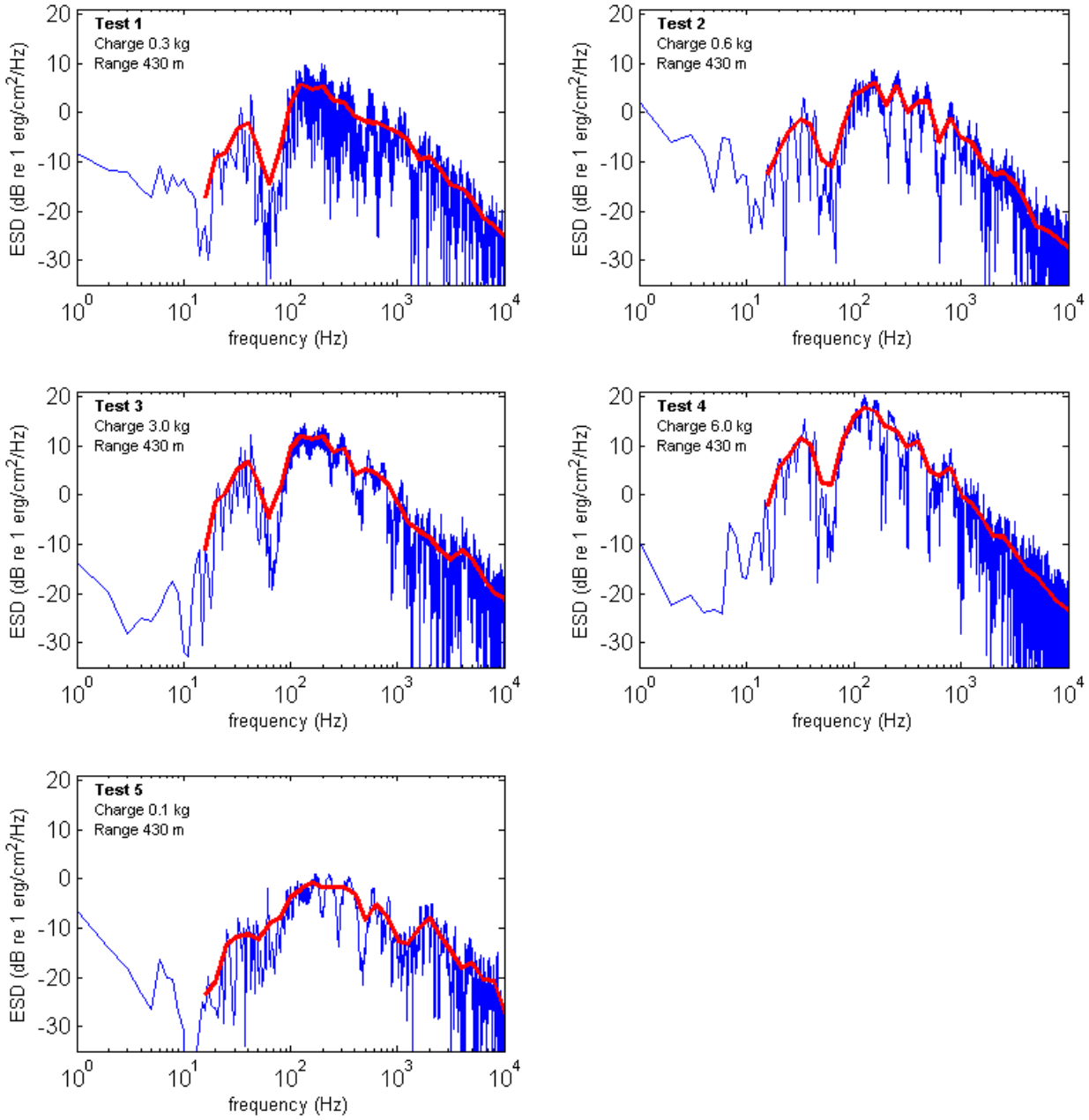

Figure 10: Energy spectral density (blue) and third-octave spectral smoothing (red) recorded from Vessel 1 on VLA Hydrophone 1. Charge weights identified in the figures represent TNT-equivalent weights.

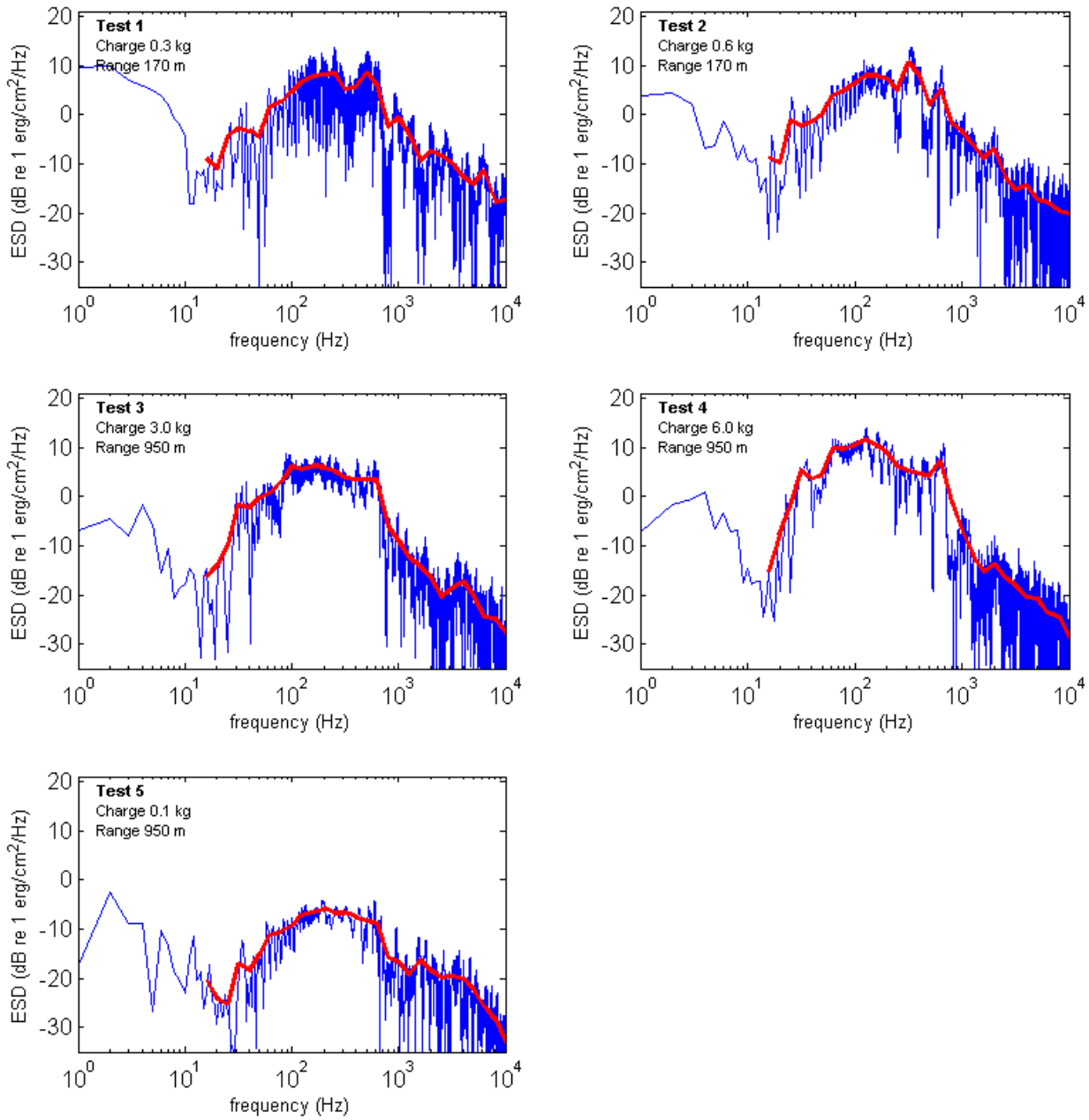

Figure 11: Energy spectral density (blue) and third-octave spectral smoothing (red) recorded from Vessel 2 on the Loggerhead. Weights identified in the figures represent TNT-equivalent weights.

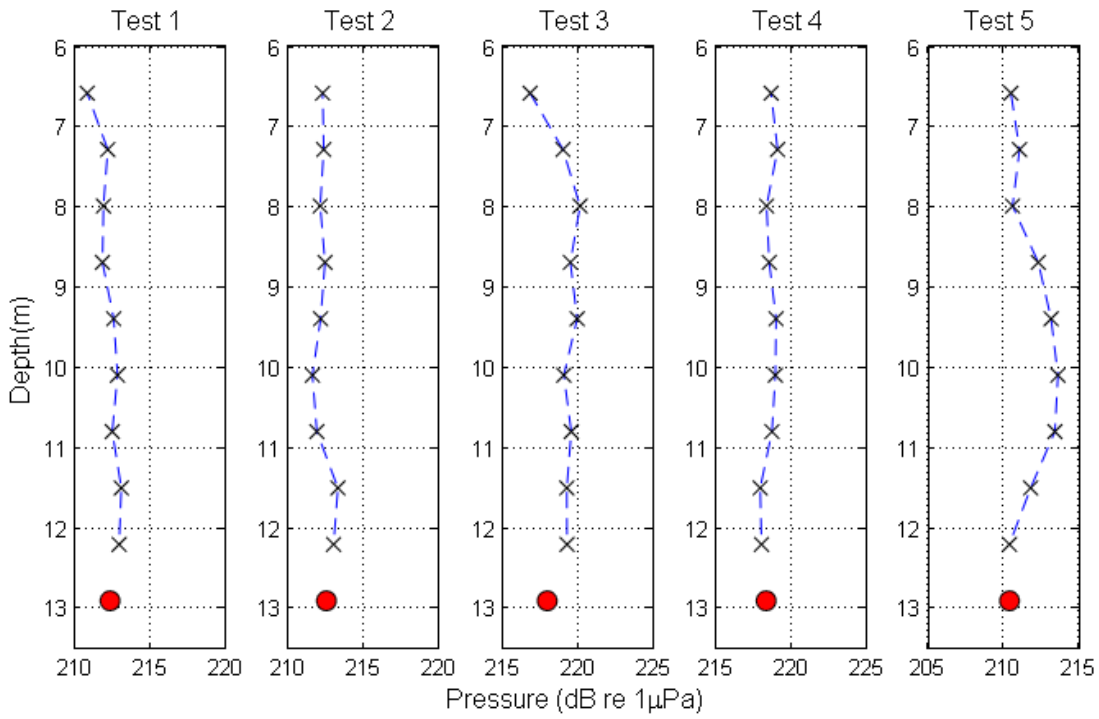

Figure 12: Depth dependence of the peak pressure for tests 1-5. VLA data are identified in black, and Loggerhead data are shown in red.

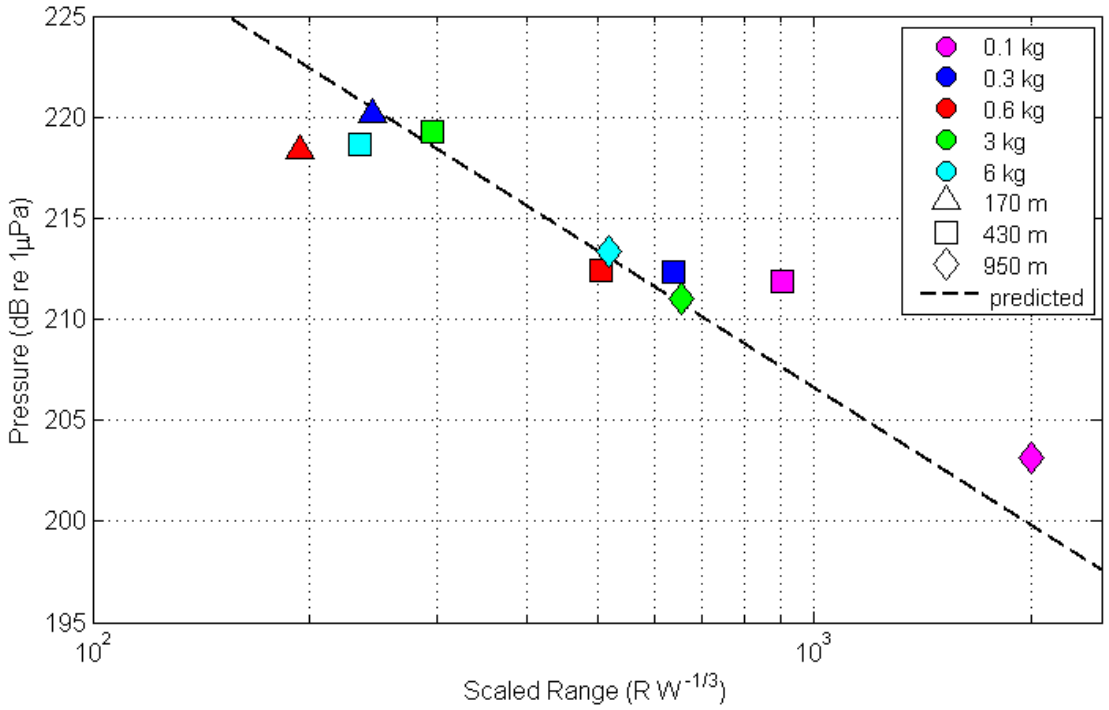

Figure 13: Peak pressure measurements plotted against scaled range ($R\,W^{-1/3}$) for Vessels 1 and 2 are shown with the predicted peak pressure from Equation 1 (black line). The marker color gives the corresponding charge weight in kg-TNT, and the marker shape identifies the measurement range.

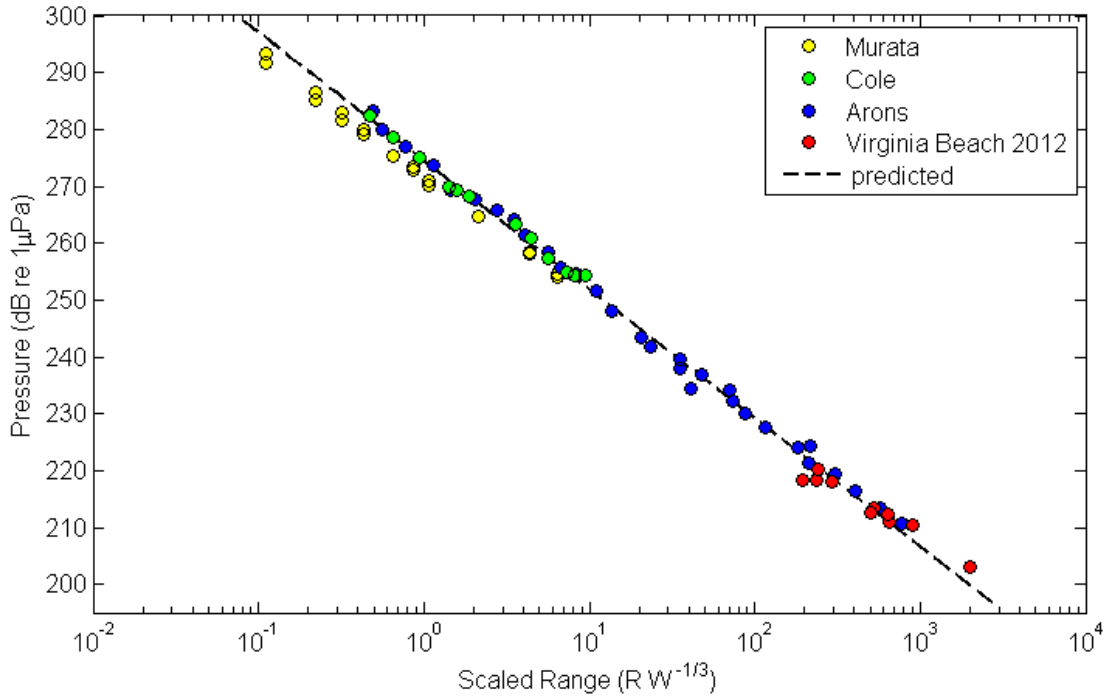

Figure 14: Peak Pressure from Virginia Beach MINEX trial, and previous measurements of Murata et al. [9], Cole [19], and Arons [1] are plotted against levels predicted by Equation 1.

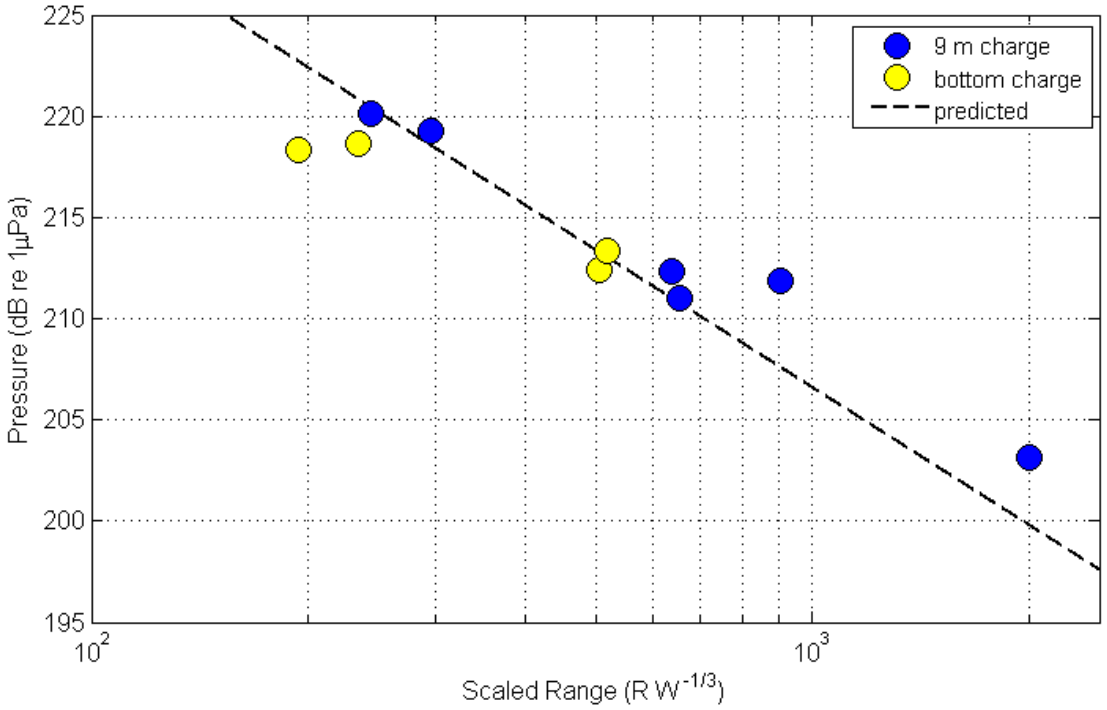

Figure 15: Peak pressure measurements identified by charge depth plotted against levels predicted by Equation 1.

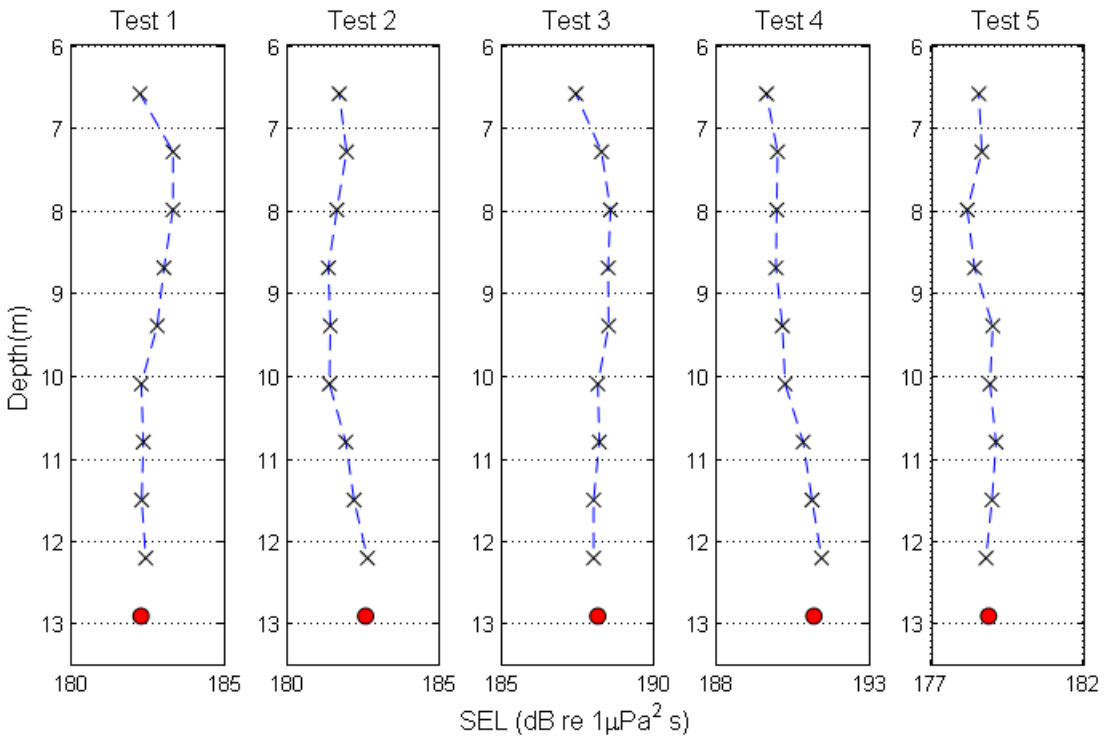

Figure 16: Depth dependence of SEL_{90} recorded from Vessel 1. VLA data indicated in black, and Loggerhead data indicated by red marker.

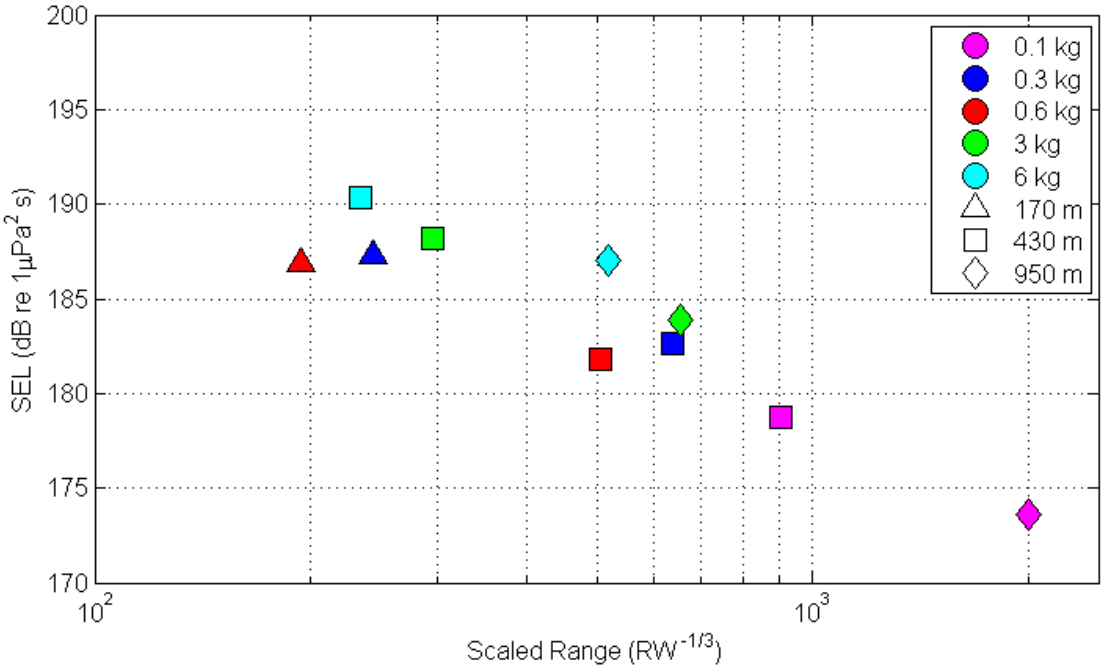

Figure 17: SEL_{90} for Vessels 1 and 2 plotted against scaled range ($R\,W^{-1/3}$). The marker color gives the corresponding charge weight in kg-TNT, and the marker shape identifies the measurement range.

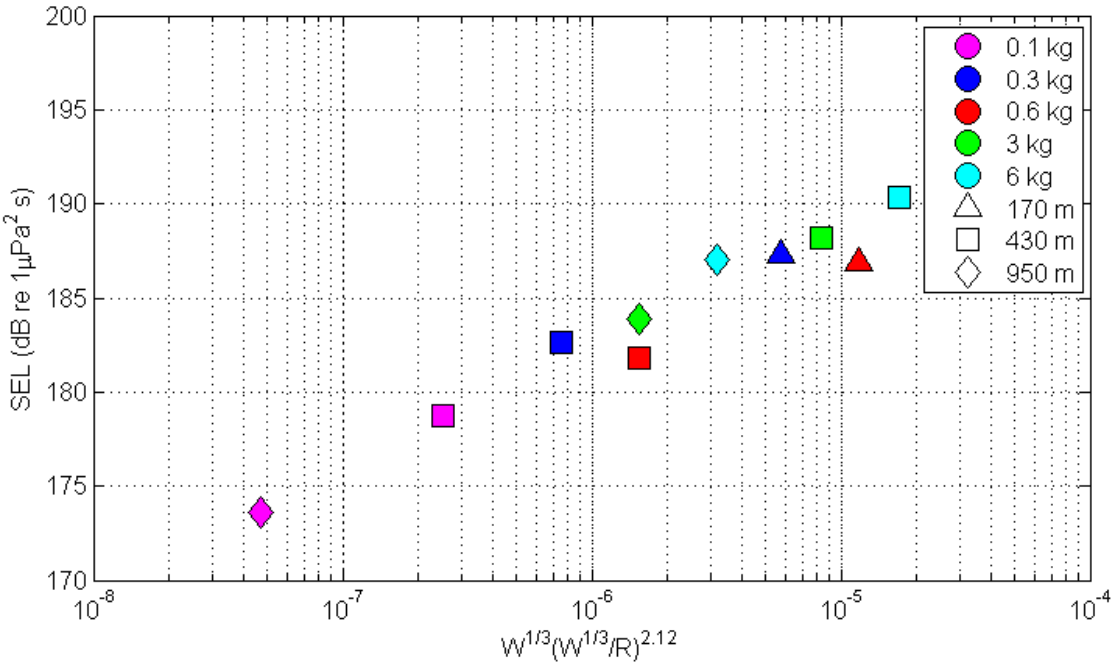

Figure 18: SEL_{90} for Vessels 1 and 2 plotted against range scaling from the empirical equation for energy flux density. The marker color gives the corresponding charge weight in kg-TNT, and the marker shape identifies the measurement range.

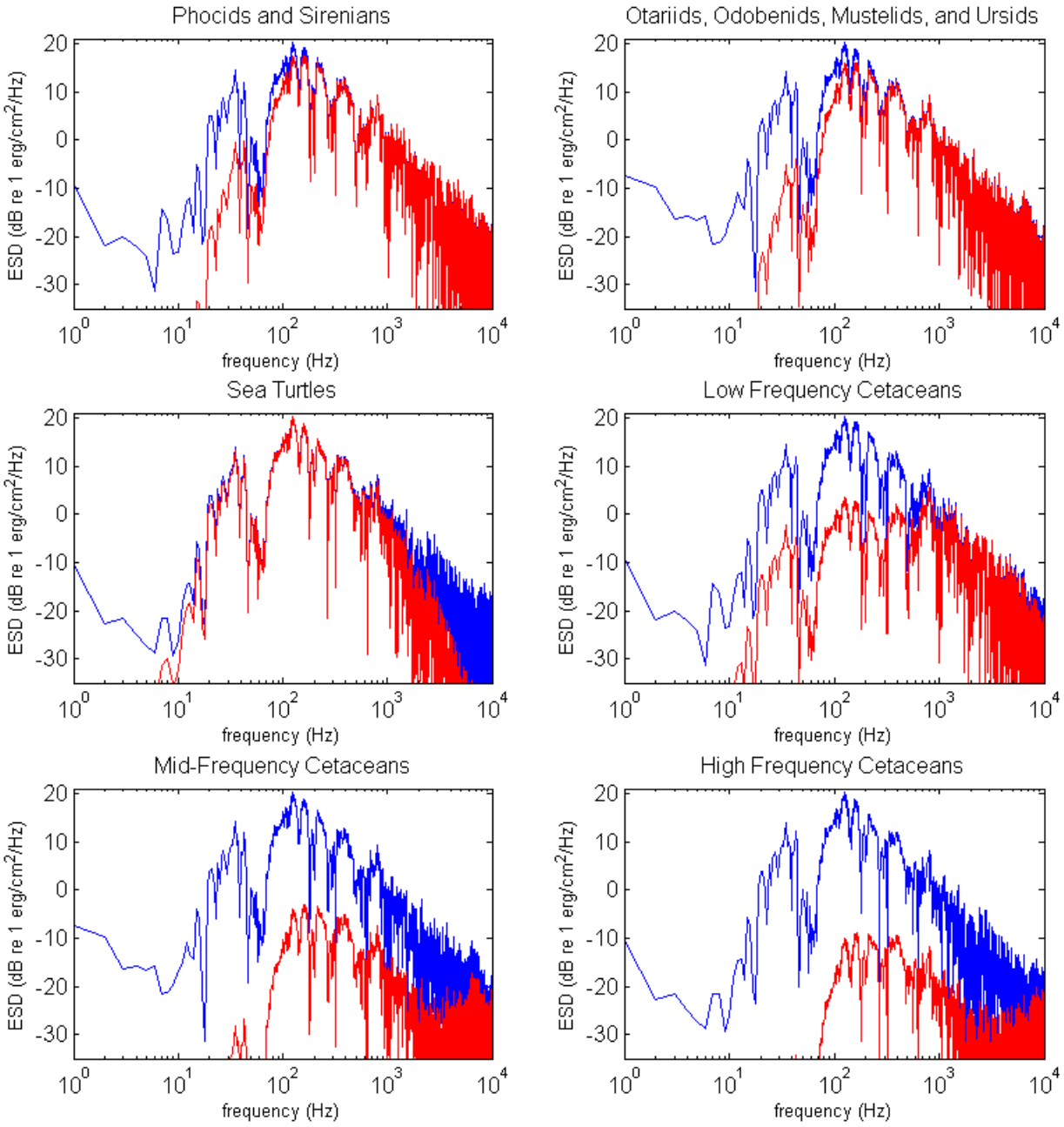

Figure 19: ESD for un-weighted measurement (blue) and measurements weighted by the functional hearing groups weighting function (red). ESD for Test 4 measurements recorded from Vessel 1 (range 430 m) on hydrophone 1 of the VLA.

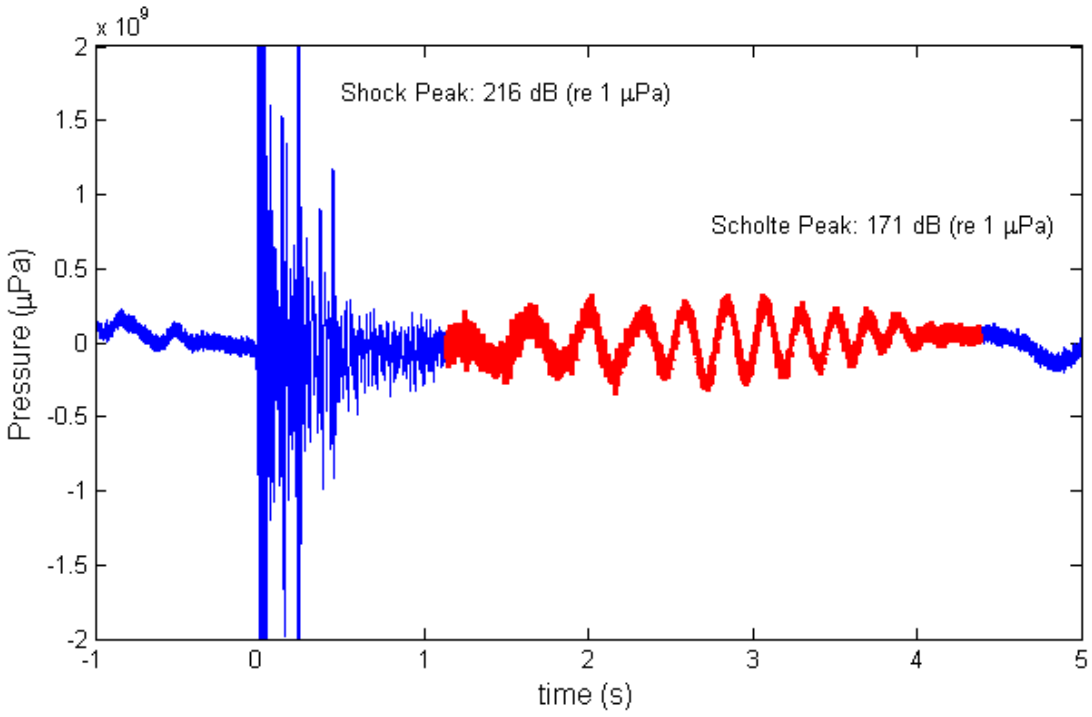

Figure 20: Test 3 time history with Scholte wave arrival indicated in red. The peak pressure for the shock arrival and the Scholte wave are also shown.

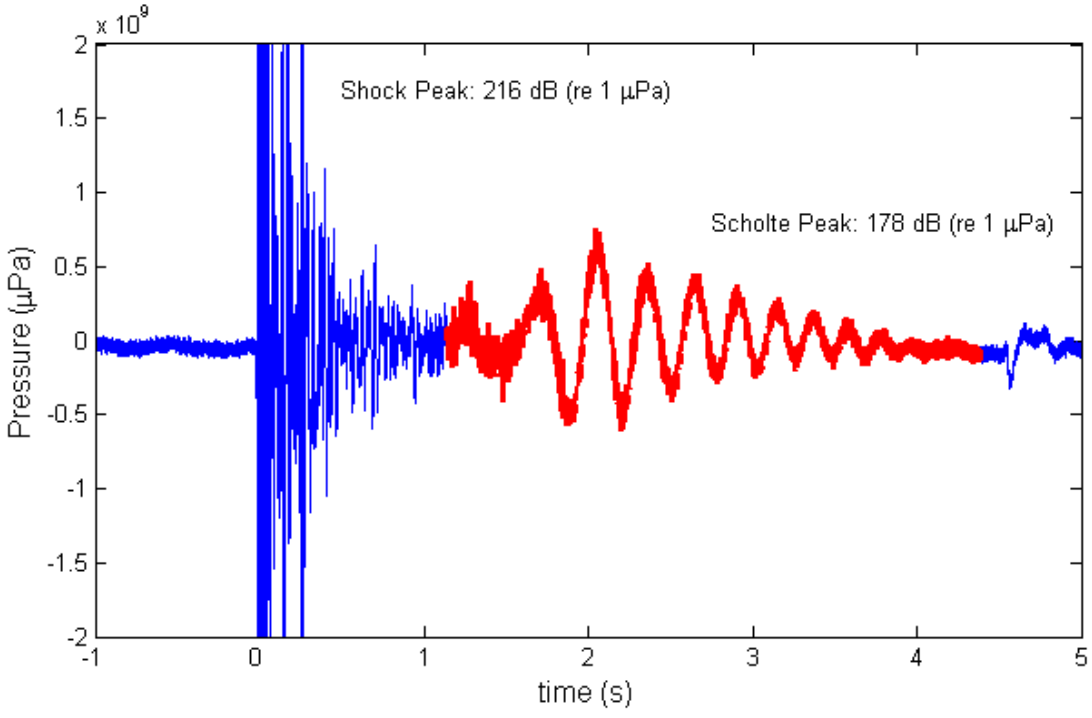

Figure 21: Test 4 time history with Scholte wave arrival indicated in red. The peak pressure for the shock arrival and the Scholte wave are also shown.

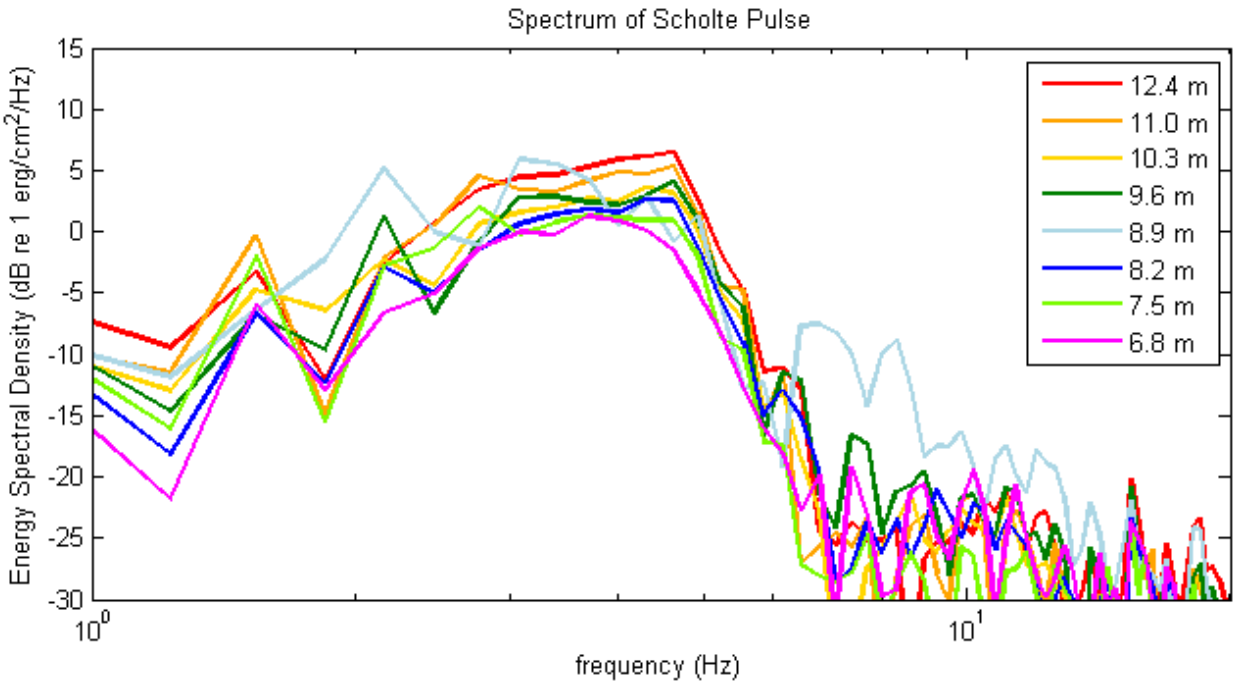

Figure 22: Energy spectral density of the Scholte wave recorded from Vessel 1 on the VLA during Test 3.

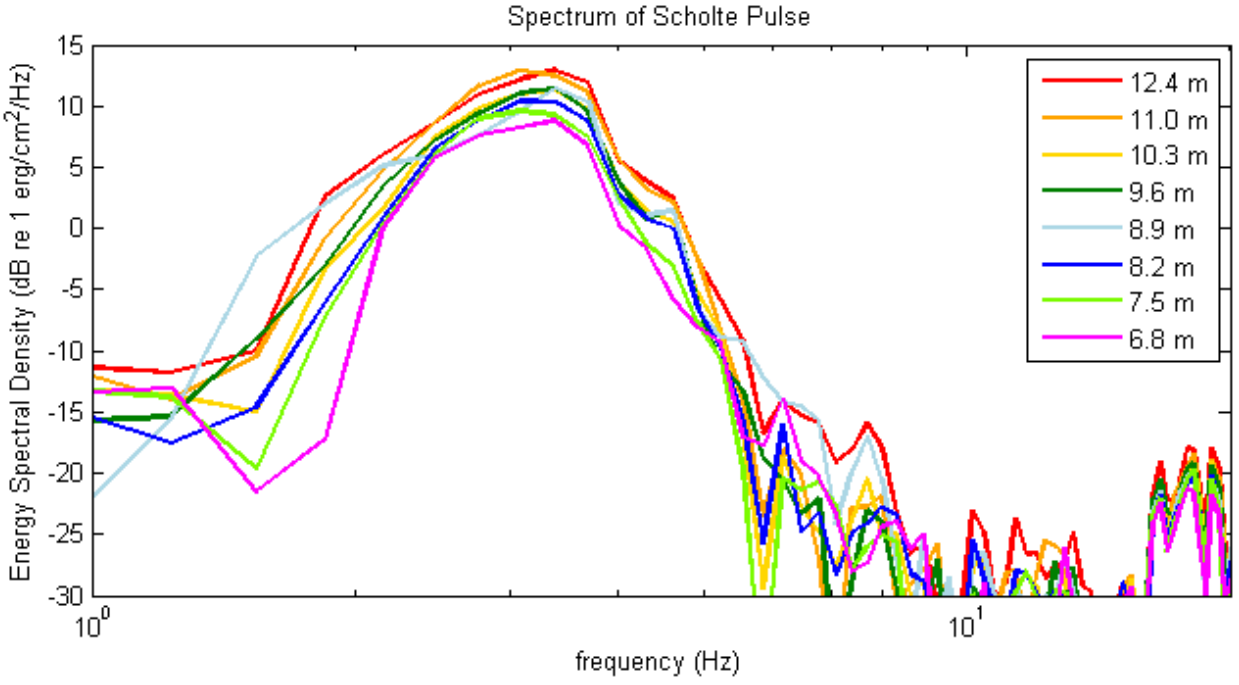

Figure 23: Energy spectral density of the Scholte wave recorded from Vessel 1 on the VLA during Test 4.

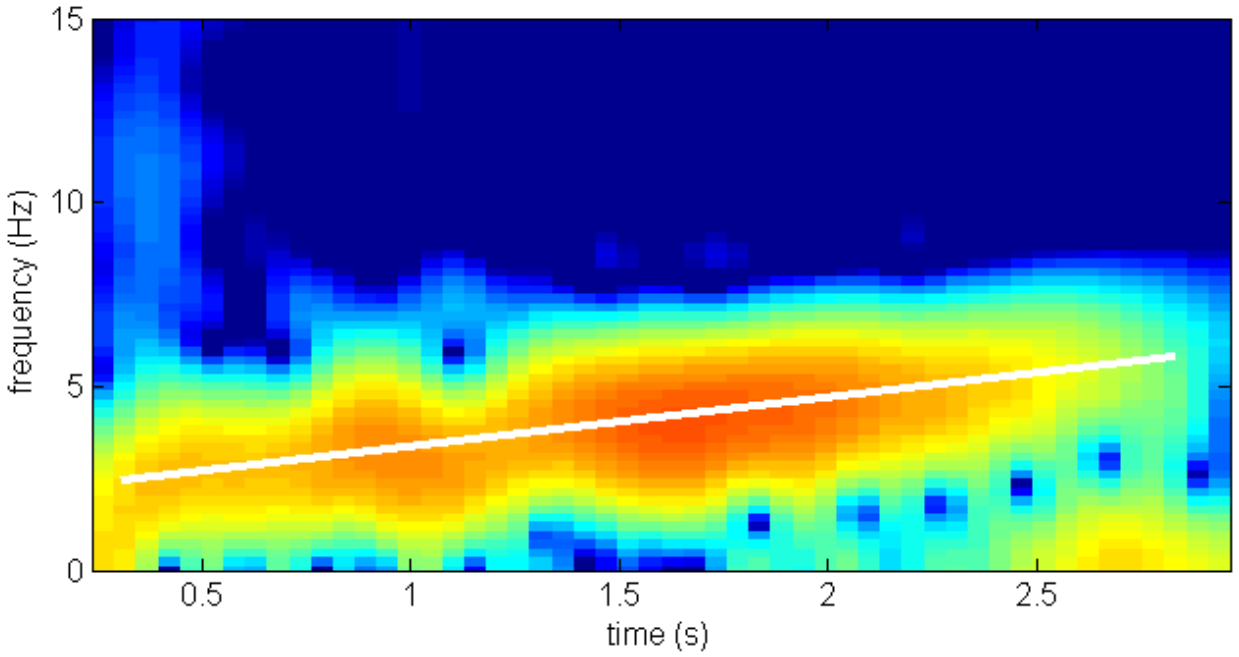

Figure 24: Spectrogram of the Scholte wave recorded during Test 3 from Vessel 1 on hydrophone 1 of the VLA. The white line indicates the dispersion trend.

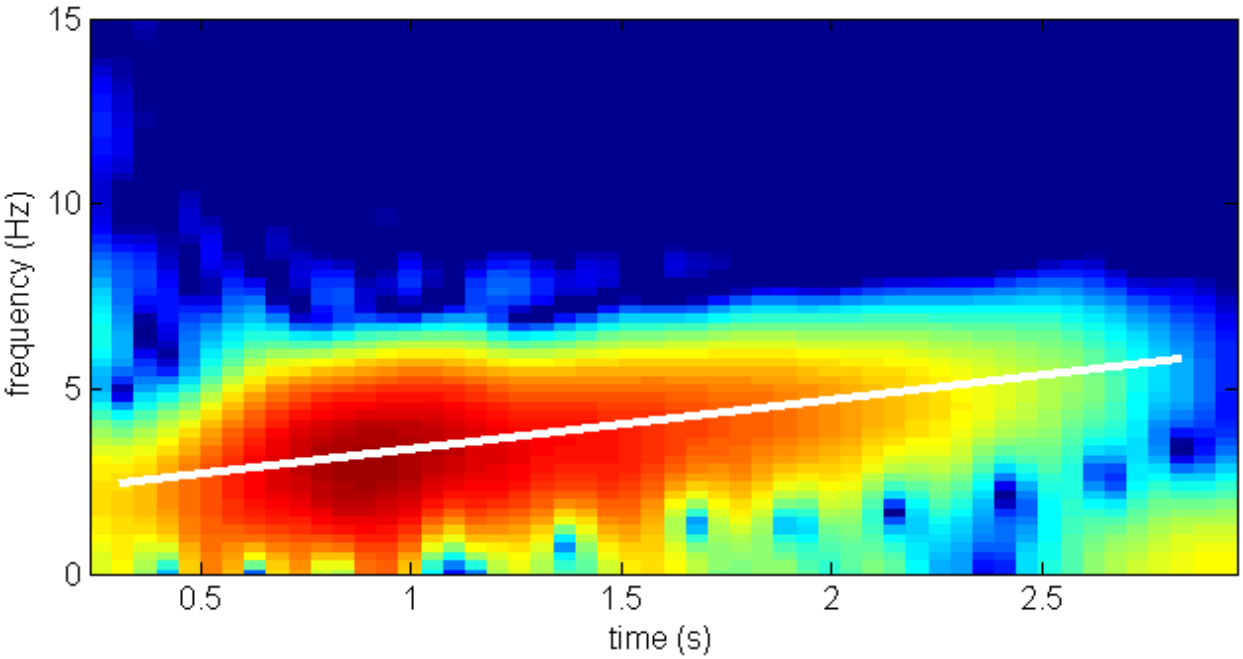

Figure 25: Spectrogram of the Scholte wave recorded during Test 4 from Vessel 1 on hydrophone 1 of the VLA. The white line indicates the dispersion trend.

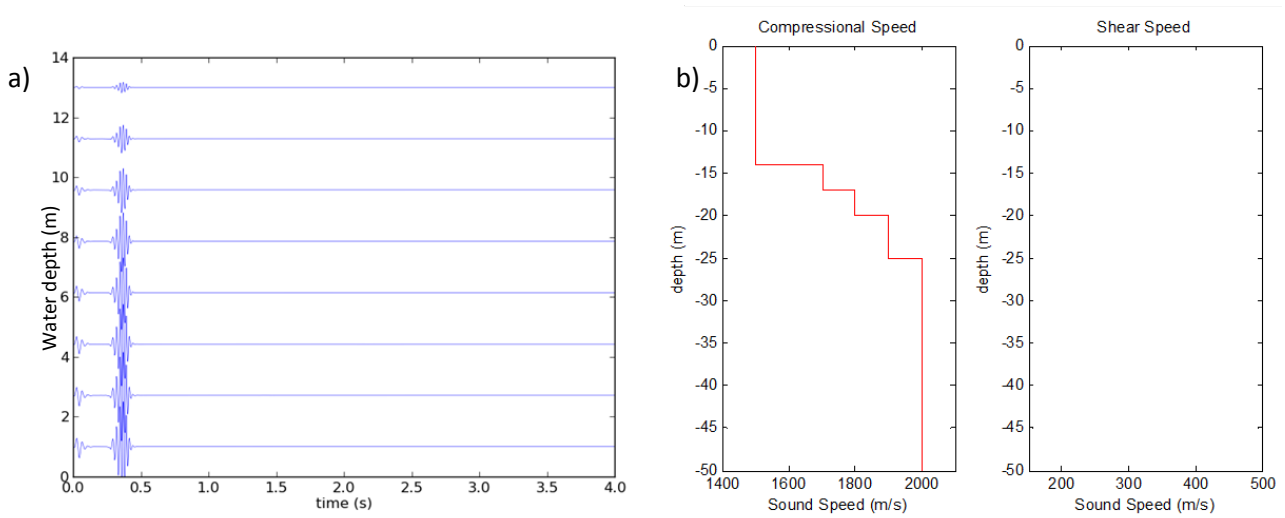

Figure 26: a) Results of OASES run of geo-acoustic model with layered bottom that does not support shear, and b) the corresponding compressional and shear speed in the sediment (not relevant for bottom that does not support shear). Zero water depth identifies the water-sediment interface, positive depths indicate the water, and negative depths indicate the sediment.

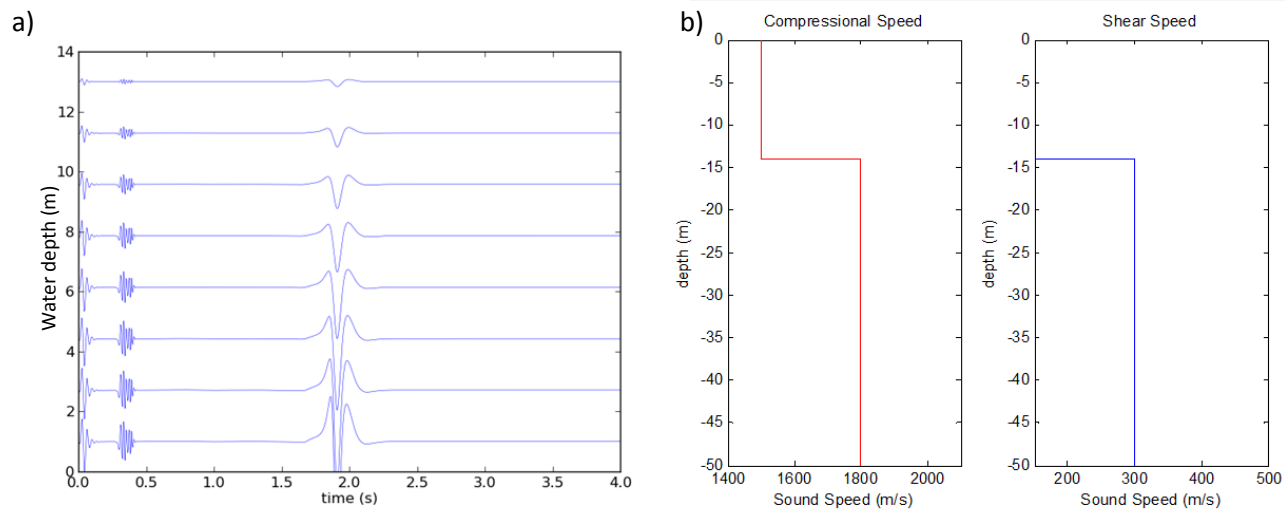

Figure 27: Results of OASES run of geo-acoustic model with single layer, shear-supporting, homogeneous bottom, and b) the corresponding compressional and shear speed in the sediment. Zero water depth identifies the water-sediment interface, positive depths indicate the water, and negative depths indicate the sediment.

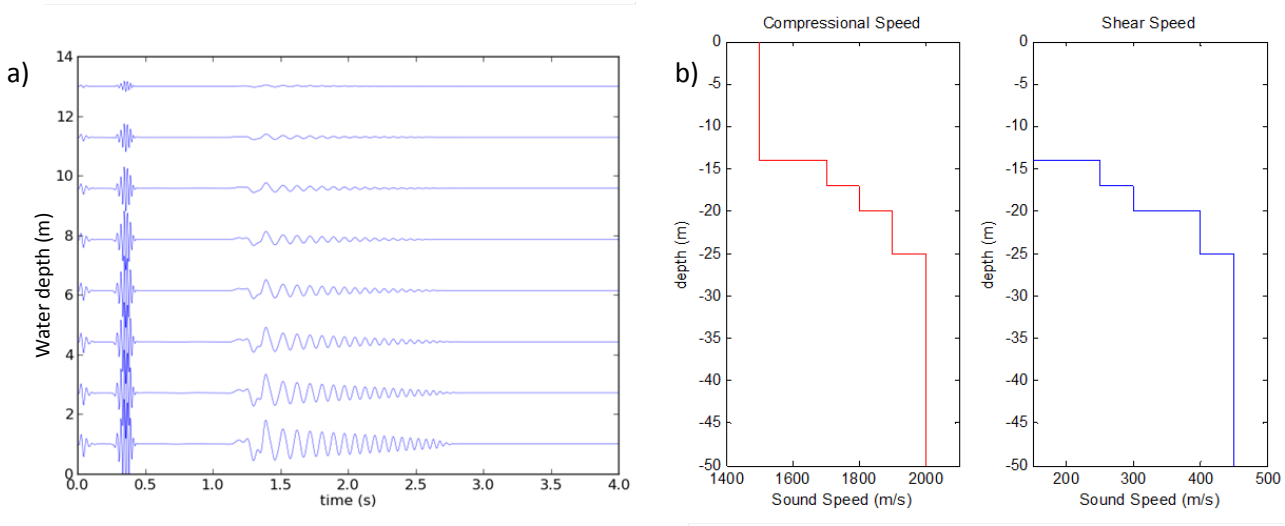

Figure 28: Results of OASES run of geo-acoustic model of layered, shear-supporting, homogeneous bottom, and b) the corresponding compressional and shear speed in the sediment. Zero water depth identifies the water-sediment interface, positive depths indicate the water, and negative depths indicate the sediment.

9. TABLES

Table 1: Summary of the functional hearing groups and auditory frequency range.

Functional Hearing Group	Sample of Functional Hearing Group Species	Auditory Frequency Range (Hz)
Low-frequency Cetaceans	North Atlantic right whale, humpback whale	7–22,000
Mid-frequency Cetaceans	Bottlenose dolphin, killer whale, pilot whale	150–160,000
High-frequency Cetaceans	harbor porpoise, river dolphin	200–180,000
Phocids Sirenians	earless seal manatees, dugong	75–75,000
Otariids Odobenids Mustelids Ursids	eared seal walrus sea otter polar bear	100–50,000
Sea Turtles	Loggerhead turtle	100–1,000

Table 2: Test charge summary.

Test	Local Time	Water Depth (m)	Explosive	Charge Depth	Charge Weight (Kg)	TNT Equivalent	TNT Equivalent Weight
1	11:04:09	15.0	C-4	9 m	0.2	1.34	0.3
2	11:12:02	15.0	C-4	Bottom	0.6	1.34	0.6
3	12:49:51	14.8	C-4	9 m	2.3	1.34	3
4	13:09:34	14.7	C-4	Bottom	4.5	1.34	6
5	16:11:59	14.7		9 m	0.07	1.50	0.1

Table 3: Depth summary of hydrophones and Hobo data loggers for Vessel 1 and Vessel 2.

Vessel 1 Hydrophone Depth (m)					
	Test 1	**Test 2**	**Test 3**	**Test 4**	**Test 5**
Hydrophone 9	6.6	6.6	6.8	6.8	6.8
Hydrophone 8	7.3	7.3	7.5	7.5	7.5
Hydrophone 7	8.0	8.0	8.2	8.2	8.2
Hydrophone 6	8.7	8.7	8.9	8.9	8.9
Hydrophone 5	9.4	9.4	9.6	9.6	9.6
Hydrophone 4	10.1	10.1	10.3	10.3	10.3
Hydrophone 3	10.8	10.8	11.0	11.0	11.0
Hobo	11.1	11.2	11.3	11.3	11.4
Hydrophone 2	11.5	11.5	11.7	11.7	11.7
Hydrophone 1	12.2	12.2	12.4	12.4	12.4
Loggerhead	12.9	12.9	13.1	13.1	13.1
Vessel 2 Hydrophone Depth (m)					
	Test 1	**Test 2**	**Test 3**	**Test 4**	**Test 5**
Loggerhead	9.5	9.7	10.0	10.4	10.3
Hobo	12.1	12.3	12.7	13.0	13.0

Table 4: Frequency below which 90 percent of the total waveform energy is contained

	Test 1	**Test 2**	**Test 3**	**Test 4**	**Test 5**
F_{90} (Hz)	2,518	2,149	1,441	978	4,865

Table 5: Measured and predicted bubble pulse periods.

Bubble Pulse Period (s)					
	Test 1	**Test 2**	**Test 3**	**Test 4**	**Test 5**
Measured	0.116	0.115	0.235	0.256	0.121
Predicted	0.121	0.125	0.260	0.269	0.085

Table 6: Charge depths calculated (second row) from measured bubble pulse period. Values in first row within parenthesis is the nominal detonation depth provided by navy.

Calculated Detonation Depth (m)				
Test 1 (9 m)	**Test 2 (Bottom)**	**Test 3 (9 m)**	**Test 4 (Bottom)**	**Test 5 (9 m)**
10.1	16.8	11.6	15.7	2.5

APPENDIX A:

TABULATED DATA

This page intentionally left blank.

Appendix A: Tabulated Data

Table A1: Summary of the peak pressure, bubble pulse period, SEL_{90} and SEL_{100} for Tests 1-5. Peak pressure and SEL for Vessel 1 are shown as a single average across the 9 VLA hydrophones.

	Peak Pressure (dB re 1µPa)		Bubble Pulse Period (s)		SEL90 (dB re $1\mu Pa^2$ s)		SEL100 (dB re $1\mu Pa^2$ s)	
	Vessel 1	Vessel 2	Vessel 1	Vessel 2	Vessel 1	Vessel 2	Vessel 1	Vessel 2
Test 1	213	220	0.116		183	187	184	188
Test 2	213	218	0.115		183	187	183	187
Test 3	220	211	0.235		188	184	189	184
Test 4	219	213	0.256		191	187	192	187
Test 5	213	203	0.121		179	173	180	174

Table A2: Depth dependence of the peak pressure as recorded from Vessel 1 on the VLA

	Peak Pressure (dB re 1 µPa)				
	Test 1	Test 2	Test 3	Test 4	Test 5
Hydrophone 1	213	213	219	218	210
Hydrophone 2	213	213	219	218	212
Hydrophone 3	213	212	220	219	213
Hydrophone 4	213	212	219	219	214
Hydrophone 5	213	212	220	219	213
Hydrophone 6	212	213	220	219	212
Hydrophone 7	212	212	220	218	211
Hydrophone 8	212	212	219	219	211
Hydrophone 9	211	212	217	219	210
Loggerhead	212	213	218	218	210

Table A3: Depth dependence of SEL_90 as recorded from Vessel 1 on the VLA

	SEL90 (dB re 1 µPa)				
	Test 1	**Test 2**	**Test 3**	**Test 4**	**Test 5**
Hydrophone 1	183	183	188	192	179
Hydrophone 2	183	183	188	192	179
Hydrophone 3	183	182	189	191	180
Hydrophone 4	183	182	189	191	179
Hydrophone 5	183	182	189	191	179
Hydrophone 6	183	182	189	190	179
Hydrophone 7	184	182	189	190	179
Hydrophone 8	184	182	189	190	179
Hydrophone 9	183	182	188	190	179
Loggerhead	183	183	188	189	179

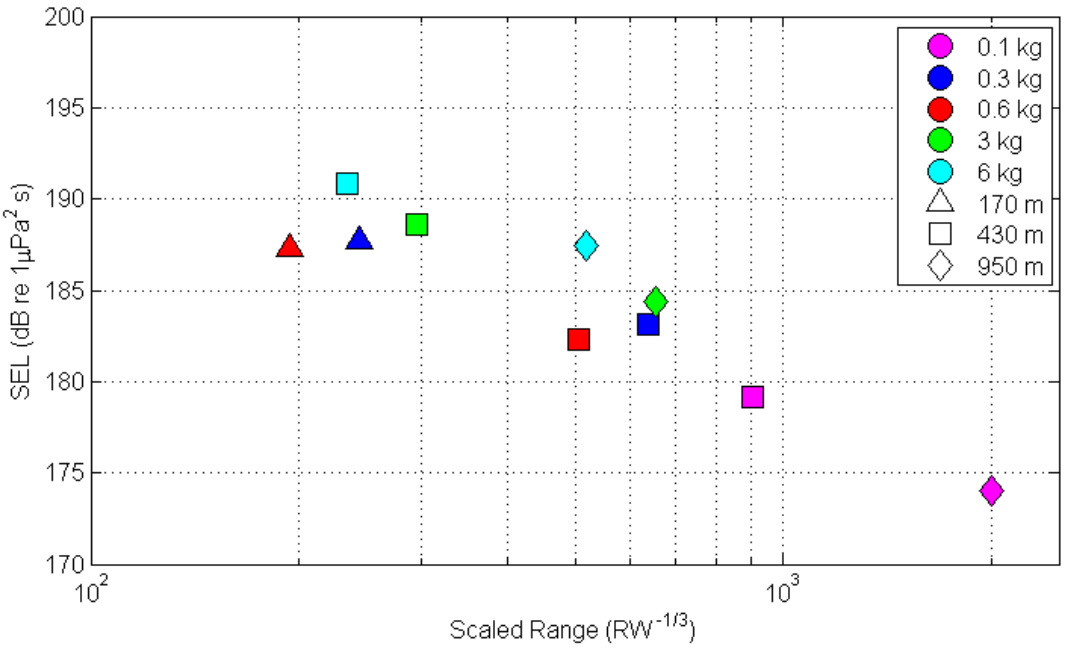

Figure A1: SEL_{100} for the Virginia Beach measurements plotted against scaled range.

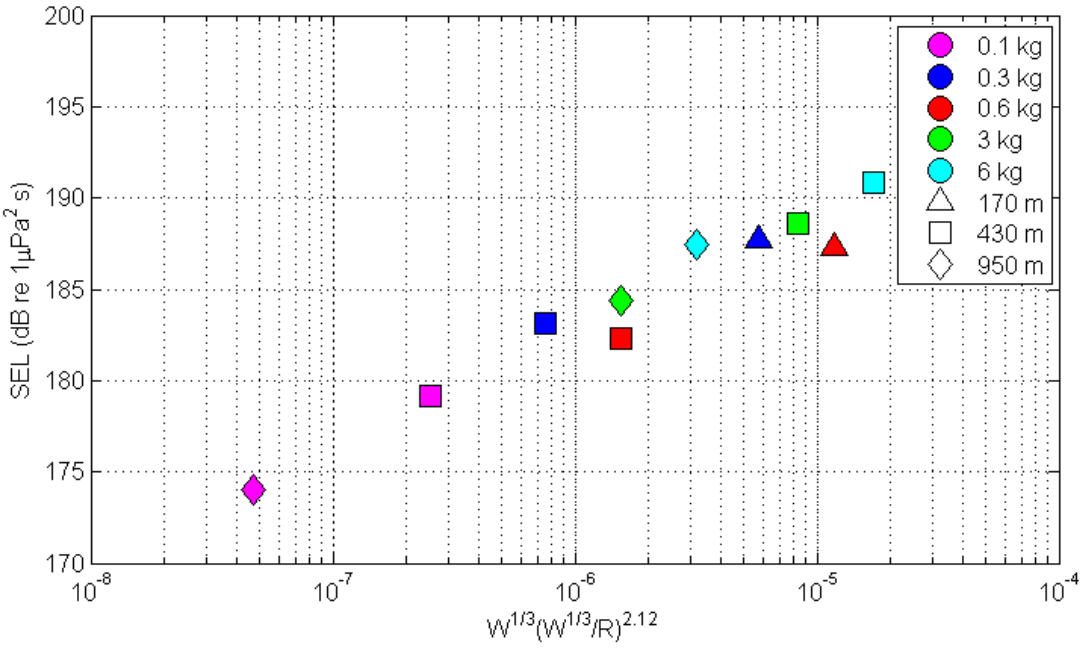

Figure A2: SEL_{100} for the Virginia Beach MINEX trial plotted against range scaling from the empirical equation for energy flux density.

This page intentionally left blank.

APPENDIX B:

NAVY EXPLOSIVES CRITERIA AND THRESHOLDS FOR MARINE MAMMALS AND SEA TURTLES

This page intentionally left blank.

Appendix B: Navy explosives criteria and thresholds for marine mammals and sea turtles

The Navy criteria and thresholds for explosives are outlined in Appendix D of "The Criteria and Thresholds for U.S. Navy Acoustic and Explosive Effects Analysis" [12]. The peak pressure and SEL_{90} calculated with auditory weighting functions are compared to the Navy criteria and thresholds (**Figures B1 and B2**). Results for SEL_{100} are also included (**Figures B3 and B4**).

Table B1: Peak Pressure and SEL_{90} for Vessel 1. Levels that exceed thresholds are identified in red.

		GI Tract Injury	PTS Threshold		TTS Threshold		Behavioral Threshold
		(unweighted) Peak SPL dB re 1 µPa	SEL90 dB re 1 µPa^2 s	(unweighted) Peak SPL dB re 1 µPa	SEL90 dB re 1 µPa^2 s	(unweighted) Peak SPL dB re 1 µPa	SEL90 dB re 1 µPa^2 s
LF Cetaceans	Navy Criteria and Threshold	237	187 (Type II)	230	172 (Type II)	224	167 (Type II)
	Test 1	212	176	212	176	212	176
	Test 2	213	176	213	176	213	176
	Test 3	218	181	218	181	218	181
	Test 4	219	182	219	182	219	182
	Test 5	210	175	210	175	210	175
MF Cetaceans	Navy Criteria and Threshold	237	187 (Type II)	230	172 (Type II)	224	167 (Type II)
	Test 1	212	167	212	167	212	167
	Test 2	213	167	213	167	213	167
	Test 3	218	172	218	172	218	172
	Test 4	219	173	219	173	219	173
	Test 5	210	167	210	167	210	167
HF Cetaceans	Navy Criteria and Threshold	237	161 (Type II)	201	146 (Type II)	195	141 (Type II)
	Test 1	212	165	212	165	212	165
	Test 2	213	165	213	165	213	165
	Test 3	218	170	218	170	218	170
	Test 4	219	171	219	171	219	171
	Test 5	210	165	210	165	210	165
Phocids, Sirenians (in water)	Navy Criteria and Threshold	237	192 (Type I)	218	177 (Type I)	212	172 (Type I)
	Test 1	212	181	212	181	212	181
	Test 2	213	182	213	182	213	182
	Test 3	218	187	218	187	218	187
	Test 4	219	190	219	190	219	190
	Test 5	210	178	210	178	210	178
Otariids, Odobenids, Mustelids, Ursids	Navy Criteria and Threshold	237	215 (Type I)	218	200	212	195
	Test 1	212	181	212	181	212	181
	Test 2	213	182	213	182	213	182
	Test 3	218	187	218	187	218	187
	Test 4	219	189	219	189	219	189
	Test 5	210	178	210	178	210	178
Sea Turtles	Navy Criteria and Threshold	237	187 (Type I)	230	172 (Type I)	224	160 (Type I)
	Test 1	212	181	212	181	212	181
	Test 2	213	182	213	182	213	182
	Test 3	218	187	218	187	218	187
	Test 4	219	191	219	191	219	191
	Test 5	210	177	210	177	210	177

Table B2: Peak Pressure and SEL_{90} for Vessel 2. Levels that exceed thresholds are identified in red.

		GI Tract Injury	PTS Threshold		TTS Threshold		Behavioral Threshold
		(unweighted) Peak SPL dB re 1 µPa	SEL90 dB re 1 µPa^2 s	(unweighted) Peak SPL dB re 1 µPa	SEL90 dB re 1 µPa^2 s	(unweighted) Peak SPL dB re 1 µPa	SEL90 dB re 1 µPa^2 s
LF Cetaceans	Navy Criteria and Threshold	237	187 (Type II)	230	172 (Type II)	224	167 (Type II)
	Test 1	220	181	220	181	220	181
	Test 2	219	179	219	179	219	179
	Test 3	211	176	211	176	211	176
	Test 4	213	178	213	178	213	178
	Test 5	203	169	203	169	203	169
MF Cetaceans	Navy Criteria and Threshold	237	187 (Type II)	230	172 (Type II)	224	167 (Type II)
	Test 1	220	173	220	173	220	173
	Test 2	219	172	219	172	219	172
	Test 3	211	167	211	167	211	167
	Test 4	213	169	213	169	213	169
	Test 5	203	160	203	160	203	160
HF Cetaceans	Navy Criteria and Threshold	237	161 (Type II)	201	146 (Type II)	195	141 (Type II)
	Test 1	220	171	220	171	220	171
	Test 2	219	170	219	170	219	170
	Test 3	211	164	211	164	211	164
	Test 4	213	165	213	165	213	165
	Test 5	203	158	203	158	203	158
Phocids, Sirenians (in water)	Navy Criteria and Threshold	237	192 (Type I)	218	177 (Type I)	212	172 (Type I)
	Test 1	220	187	220	187	220	187
	Test 2	219	186	219	186	219	186
	Test 3	211	183	211	183	211	183
	Test 4	213	186	213	186	213	186
	Test 5	203	173	203	173	203	173
Otariids, Odobenids, Mustelids, Ursids	Navy Criteria and Threshold	237	215 (Type I)	218	200	212	195
	Test 1	220	186	220	186	220	186
	Test 2	219	186	219	186	219	186
	Test 3	211	183	211	183	211	183
	Test 4	213	185	213	185	213	185
	Test 5	203	173	203	173	203	173
Sea Turtles	Navy Criteria and Threshold	237	187 (Type I)	230	172 (Type I)	224	160 (Type I)
	Test 1	220	186	220	186	220	186
	Test 2	219	186	219	186	219	186
	Test 3	211	183	211	183	211	183
	Test 4	213	187	213	187	213	187
	Test 5	203	172	203	172	203	172

Table B3: Peak Pressure and SEL_{100} for Vessel 1. Levels that exceed thresholds are identified in red.

		GI Tract Injury	PTS Threshold		TTS Threshold		Behavioral Threshold
		(unweighted) Peak SPL dB re 1 µPa	SEL100 dB re 1 µPa^2 s	(unweighted) Peak SPL dB re 1 µPa	SEL100 dB re 1 µPa^2 s	(unweighted) Peak SPL dB re 1 µPa	SEL100 dB re 1 µPa^2 s
LF Cetaceans	Navy Criteria and Threshold	237	187 (Type II)	230	172 (Type II)	224	167 (Type II)
	Test 1	212	177	212	177	212	177
	Test 2	213	177	213	177	213	177
	Test 3	218	181	218	181	218	181
	Test 4	219	182	219	182	219	182
	Test 5	210	176	210	176	210	176
MF Cetaceans	Navy Criteria and Threshold	237	187 (Type II)	230	172 (Type II)	224	167 (Type II)
	Test 1	212	168	212	168	212	168
	Test 2	213	168	213	168	213	168
	Test 3	218	173	218	173	218	173
	Test 4	219	174	219	174	219	174
	Test 5	210	167	210	167	210	167
HF Cetaceans	Navy Criteria and Threshold	237	161 (Type II)	201	146 (Type II)	195	141 (Type II)
	Test 1	212	166	212	166	212	166
	Test 2	213	165	213	165	213	165
	Test 3	218	170	218	170	218	170
	Test 4	219	171	219	171	219	171
	Test 5	210	165	210	165	210	165
Phocids, Sirenians (in water)	Navy Criteria and Threshold	237	192 (Type I)	218	177 (Type I)	212	172 (Type I)
	Test 1	212	182	212	182	212	182
	Test 2	213	182	213	182	213	182
	Test 3	218	188	218	188	218	188
	Test 4	219	190	219	190	219	190
	Test 5	210	179	210	179	210	179
Otariids, Odobenids, Mustelids, Ursids	Navy Criteria and Threshold	237	215 (Type I)	218	200	212	195
	Test 1	212	181	212	181	212	181
	Test 2	213	182	213	182	213	182
	Test 3	218	187	218	187	218	187
	Test 4	219	190	219	190	219	190
	Test 5	210	179	210	179	210	179
Sea Turtles	Navy Criteria and Threshold	237	187 (Type I)	230	172 (Type I)	224	160 (Type I)
	Test 1	212	181	212	181	212	181
	Test 2	213	182	213	182	213	182
	Test 3	218	187	218	187	218	187
	Test 4	219	191	219	191	219	191
	Test 5	210	177	210	177	210	177

Table B4: Peak Pressure and SEL_{100} for Vessel 2. Levels that exceed thresholds are identified in red..

		GI Tract Injury	PTS Threshold		TTS Threshold		Behavioral Threshold
		(unweighted) Peak SPL dB re 1 µPa	SEL100 dB re 1 µPa^2 s	(unweighted) Peak SPL dB re 1 µPa	SEL100 dB re 1 µPa^2 s	(unweighted) Peak SPL dB re 1 µPa	SEL100 dB re 1 µPa^2 s
LF Cetaceans	Navy Criteria and Threshold	237	187 (Type II)	230	172 (Type II)	224	167 (Type II)
	Test 1	220	182	220	182	220	182
	Test 2	219	180	219	180	219	180
	Test 3	211	176	211	176	211	176
	Test 4	213	179	213	179	213	179
	Test 5	203	170	203	170	203	170
MF Cetaceans	Navy Criteria and Threshold	237	187 (Type II)	230	172 (Type II)	224	167 (Type II)
	Test 1	220	174	220	174	220	174
	Test 2	219	173	219	173	219	173
	Test 3	211	167	211	167	211	167
	Test 4	213	169	213	169	213	169
	Test 5	203	160	203	160	203	160
HF Cetaceans	Navy Criteria and Threshold	237	161 (Type II)	201	146 (Type II)	195	141 (Type II)
	Test 1	220	172	220	172	220	172
	Test 2	219	171	219	171	219	171
	Test 3	211	164	211	164	211	164
	Test 4	213	166	213	166	213	166
	Test 5	203	158	203	158	203	158
Phocids, Sirenians (in water)	Navy Criteria and Threshold	237	192 (Type I)	218	177 (Type I)	212	172 (Type I)
	Test 1	220	187	220	187	220	187
	Test 2	219	187	219	187	219	187
	Test 3	211	183	211	183	211	183
	Test 4	213	186	213	186	213	186
	Test 5	203	174	203	174	203	174
Otariids, Odobenids, Mustelids, Ursids	Navy Criteria and Threshold	237	215 (Type I)	218	200	212	195
	Test 1	220	187	220	187	220	187
	Test 2	219	186	219	186	219	186
	Test 3	211	183	211	183	211	183
	Test 4	213	186	213	186	213	186
	Test 5	203	173	203	173	203	173
Sea Turtles	Navy Criteria and Threshold	237	187 (Type I)	230	172 (Type I)	224	160 (Type I)
	Test 1	220	186	220	186	220	186
	Test 2	219	186	219	186	219	186
	Test 3	211	184	211	184	211	184
	Test 4	213	187	213	187	213	187
	Test 5	203	172	203	172	203	172

This page intentionally left blank.

APPENDIX C:

ADDITIONAL DATA DISTRIBUTION AND USAGE

This page intentionally left blank.

Appendix C: Additional Data Distribution and Usage

The data collected during the Virginia Beach MINEX trial have been distributed as follows;

1. At their request, portions of the data were supplied to NUWC Division Newport, Code 70 (P.O.C. Peter Hulton) in March 2013 for use in testing of the NUWC REFEMS explosive simulation model

2. At their request, portions of the data were supplied to Applied Physical Sciences Corp. (P.O.C. Kevin Cockrell) in January 2014 for their validation of mine detection/classification algorithms as funded by ONR/NAVSEA

3. The data continue to be analyzed by Alexander G. Soloway as part of his MSME thesis at the University of Washington. Some or all of the content of this report will appear in the completed thesis.

This page intentionally left blank.